POLYCHROMATIC MICRO X-RAY BEAM STRAIN ANALYSIS OF ALUMINUM SAPPHIRE COMPOSITE

By

HRISHIKESH BALE

Bachelor of Engineering
Visveswaraiah Technological University
Belgaum, Karnataka, India.
(August 2002)

Submitted to the Faculty of the
Graduate College of the
Oklahoma State University
In partial fulfillment of
the requirements for
the Degree of
MASTER OF SCIENCE
December, 2005

POLYCHROMATIC MICRO X-RAY BEAM STRAIN
ANALYSIS OF ALUMINUM
SAPPHIRE COMPOSITE

Thesis approved:

Dr. Jay C. Hanan
Thesis Advisor

Dr. C.E. Price

Dr. Demir Coker

Dr. A. Gordon Emslie
Dean of the Graduate College

ACKNOWLEDGMENTS

I am highly indebted to my father Mr. Ashok Bale and mother Mrs. Ashwini Bale for continuously providing me with the high motivation and encouragement to achieve success. My sisters, Gauri and Girija have always been a great help, pouring in huge amount of valuable inputs. I would like to thank my aunt Dr. Kala Pant, a perfectionist and achiever who has always been an inspiration. Special thanks are due to my roommates and friends who always had an ever-present support during the entire Master's program.

I am very thankful to my adviser Dr. Jay Hanan for guiding me through a long way. Dr. Hanan has always been a high source of inspiration for me in every aspect. I greatly appreciate the help he has offered me in learning some of the interesting subjects which are surely huge milestones, I had never imagined. It definitely makes me proud to be Dr. Hanan's first graduate student and would like to thank him for offering me such a chance.

I wish to express my sincere appreciation to Dr. C.E. Price and Dr. Hongbing Lu for providing invaluable guidance and encouragement throughout this study. I would also like to thank Dr. Ghajar for his help and guidance. I wish to specially thank Dr. R. D. Delahoussaye for helping me with valuable suggestions and financial support during the course of my first year at OSU.

I wish to express my gratitude to The Director of The Advanced Light Source, Office of Science, Office of Basic Energy Sciences, of the U.S. Department of Energy under Contract No. DE-AC02-05CH11231. I am deeply indebted to Dr. Nobumichi Tamura for providing me with his valuable software code which has led me all the way in my research.

My sincere thanks to Chris Teed, of Accu-Wire EDM, for the portion of sample preparation which involved Electro-Discharge Machining (EDM).

Special thanks to Abhijeet Utturkar, for continuously suggesting valuable ideas which have contributed a lot to the current work. Last but not the least, I would specially thank Amol Birje, Amol Ganpatye, Bharat Joshi, Abhijeet Barve, Mayuresh Kulkarni and Saurabh Pawar for their huge support in this effort.

Table of Contents

Chapter **Page**

List of Figures

Figure **Page**

CHAPTER 1

1.0 INTRODUCTION

The modern era of material science deals with newer and specialized materials with enhanced properties. Among them composites are a major constituent with key features such as high strength, light weight and versatility. To achieve such highly enhanced properties as high specific strength and specific modulus, and maintain toughness in materials, a combination of different materials is required. Among a huge variety of composites that are in use today, one important type is the metal matrix composite (MMC). MMC's often consist of metal or alloy matrix with reinforcing ceramic fibers.

Metal matrix composites (MMC's) were introduced as structural materials in the early 1970s. There has been tremendous development of MMC's since then which has led to its transition from being a mere laboratory research material to a wide scale commercialized structural material due to its special applicability. MMC's have become the material of choice in various areas of aerospace applications, especially where high temperatures exist and where material sustainability plays a key role. Typical applications for these materials would be in engine components or hypersonic aircraft where reduced

weight and higher operating conditions offer significant performance advantages (increased engine efficiency, higher fuel economy, higher operating speeds, etc.). MMC's have also found way into the automobile industry where specific strength and weight play an important role. MMC's have replaces polymer based composites in certain areas where elevated temperatures persist, because of the inability of the polymer matrix to sustain high temperatures. Besides applications in high temperature areas MMC's are also applied when characteristics of the metal matrix such as toughness, hardness, electrical conductivity, and strength are desired. This versatility of MMC's can be attributed to the flexibility it offers to control specific properties. Developments related to the reinforcing materials have been underway which has led to MMC's with a wide variety based on the reinforcing type and material, each finding a specific application. Reinforcing materials typically consist of continuous fibers, short fibers, and also inclusions. The MMC's with continuous fiber reinforcement provides the highest structural performance. These composites utilize ceramic based fibers which inherently have a very high modulus for superior strength and rely on the matrix for the support and stress transfer between fibers. [1, 2, 3]

Unlike polymer matrix composites, very few types of micro mechanical models have been formulated for the metal matrix composites. Also there are no polymer matrix analogues for the MMC's, which best describe the mechanical behavior of the composite. Thus, formulation of new mathematical models for MMC's, which can give in-depth details of the behavior of these composites, is needed. However, complexity in mathematical modeling is increased due to geometric arrangements of the

reinforcements, coefficient of thermal expansion (CTE) mismatch, fiber-matrix bond behavior and the distribution of the strength within the fibers. [4]

One issue among MMC's highlighted here is the difference in coefficient of thermal expansion of the constituents accompanied by the specifics of the crystal structure of the individual material. There also exists a considerable difference in the Poisson's ratio and material stiffness—even within the same anisotropic crystal. The fact that such materials with widely varying characteristics are combined together to bring out superior properties itself poses certain problems such as fabrication difficulties due to characteristic properties of individual materials, varying crystallography, and many other physical parameters. Another important mechanism in the failure of composites is de-bonding of the fibers from the matrix.

With these factors under consideration, the knowledge of the effects of the residual and applied stresses on the material at a micro-structural level is highly advantageous. High energy synchrotron X-ray sources with high spatial resolution prove to be a tool in analysis of the above mentioned critical parameters in case of composites. The use of polychromatic light using Laue diffractions aids in analyzing composites at submicron levels and proves to be a non destructive way of measuring data from specimens. The measurement of strains can be precisely made to the order of 10^{-4} with this technique [5] as opposed to 10^{-3} using previous methods. The current experiment utilizes the rediscovered Laue technique in acquiring valuable information such as the residual strains and strain behavior upon loading the composites.

CHAPTER 2

2.0 MODELING OF COMPOSITES

The calculation of residual strains and stresses within a material using diffraction is well developed [6]. However the experimental determination of the actual values of the internal strains and stresses has been a challenging task, especially in materials like composites which include a variety of constituent materials. Conventional stress analysis of fiber composites employs the use of strain gage rosettes on the surface of the matrix. Test methods such as the ASTM specification D3039-76 (1990) provide a detailed example of the traditional analysis which provides information on the longitudinal and transverse tensile strength, Young's moduli, tensile strain, and major (longitudinal) and minor (transverse) Poisson's ratios.[7] These documented values are determined utilizing the combined failure of the composite, and hence individual stress-strain behavior of the matrix and the fiber is unknown. Typical composite deformation includes collective nucleation and evolution of damage, fiber fractures, matrix fractures and plasticity, as well as interface separation and sliding. Determination of the mechanical behavior of the matrix and fibers separately within the composite can provide the progression of failure in MMC's right from failure initiation starting with collective nucleation at the

reinforcement and evolution of damage, led by the fiber fractures, succeeded by the matrix failure with plastic deformation, bond failure and separation.

The ability to judge the existence of internal stresses can lead to the mechanism of the elastic as well as the plastic deformation in polycrystalline materials, as well as a variety of materials. Several non-destructive evaluation techniques have been developed to date to find the strains and stresses that exist in a component. *In-situ* measurements of stress/strain can then be used to validate and refine predictive micromechanics models [8, 9]. Among these optical techniques, ultrasound, acoustic emission monitoring, and neutron diffraction have been used [10, 11, 12, 13, 14, 15]. All of the techniques mentioned provide data which is specific to discontinuities in the medium and, in the case of fiber composites, fiber breaks are detected. With the exception of neutron diffraction, these methods do not provide quantitative strains in most materials, and with neutron diffraction spatially resolved measurements are rare [16]. In special cases, quantitative measurements have been achieved using optical methods such as micro-Raman and piezo-spectroscopy [6,14,15,17,18,19,20]. In most of these studies, either the matrix could not be characterized, or only shallow surface regions were investigated.

More general probes that measure both the matrix strain and the reinforcement strain are necessary to fully understand composite deformation. X-ray diffraction has been a technique widely used for strain measurement. Low-energy X-ray diffraction for Cu-X-ray tubes has been standardized to measure stress in many materials [6, 21]. However, for most materials, low-energy X-ray diffraction provides information specific to the

material surface. Destructive methods such as layer removal employed low-energy X-rays for depth-resolved residual strain measurements. Using Neutron diffraction in-depth studies of the bulk composite response to applied stress coupled with phase-specific fiber and matrix strains have been performed [16, 22, 23, 24, 25, 26, 27, 28, 29, 30]. Other more recent investigations have shown that the fiber matrix interface is characterized by abrupt variations in stress ignored by continuum mechanical models [31, 32]. Thus, a general lack of information concerning MMC deformation mechanisms at the scale of the microstructure persists. [3]

2.1 Modeling of the poly-crystalline phases in a composite system

Beyond the mechanical models used for composites, an examination at the micro-scale requires an understanding of the grain-grain interactions. While the bulk metal matrix may be considered mechanically isotropic, anisotropy of the individual grains must be understood to correctly interpret measurements at the grain and sub-grain level. Several mechanical models have been proposed to describe the behavior.

The simpler models such as the concentric cylinder or the Eshelby model [33] suggest fiber fraction is the more sensitive parameter determining composites properties. Previous research conducted by Sachs [34] and Taylor [35] are simple one-site models developed to study poly-crystalline materials. Also researched among the one-site model was the self consistent model [36, 37, 38, 39, 40]. In case of the one-site models, it is assumed that individual grains interact with the surrounding material continuum. This also indicates that all those grains with the same crystallographic orientation behave

identically. Later on, the poly-crystal models that were developed were n-site models [36]. This type of modeling considers that even though some grains may be crystallographically oriented identically, they can behave in different manners. Bulk properties have also been predicted with relative success using finite element modeling (FEM). Several efforts to improve computational speed over FEM have been proposed.

Models based on descriptions related to anisotropy, as proposed by Bishop and Hill [41], have been proposed which estimate the strength of a crystal undergoing deformation depending on the crystal orientation and the geometry of deformation [42, 43]. Based on the Hill-Bishop models it is found that in case of poly-crystals the strength can vary by a factor of as much as two depending on the crystal orientation. This arises mainly from the disposition of the slip systems with respect to the deformation geometry. Whatever model is employed to understand MMC's and their constituents, there still remains an overwhelming need to validate or refute the predictions with relevant mechanical data. Such data are in short supply. Modeling studies are often compared to predictions from Monte Carlo simulations [44, 45] or incomplete subsets of data [8 (p. 241)], limiting the ultimate relevance to the engineer who must deal with the real composite. Some experimental evaluation and mathematical approach towards the anisotropy existing in polycrystalline materials is considered by E. Depaolini et. al. [46]. Their work quantitatively represents the distribution of orientations of crystallites which is used in modeling poly-crystals mathematically.

CHAPTER 3

3.0 DIFFRACTION

The early use of X-rays to study materials dates back to the early nineteen hundreds when, Roentgen's discovery of X-rays in 1912, sparked enthusiasm among many crystallographers and physicists. Von Laue discovered in 1912 that crystals diffract X-rays in a unique manner which can be used to reveal the structure of the crystal. Since most engineering materials used are crystalline in nature, the use of X-rays works as a very useful tool for non-destructive analysis. The relevant order of developments that have taken place since the discovery of X-rays in 1912 has been summarized in the following chart. A broad classification is seen with two main techniques 1) X-ray diffraction and 2) Neutron Diffraction. The initial X-ray diffraction studies involved comparatively large sized beams (about 1 mm x 3 to 5mm) which were utilized to carry out surface diffraction measurements on samples. Following an outline of the historical progression to the present diffraction technique a brief explanation of the theory of Bragg's law of diffraction is presented in the succeeding text.

Measurements of strain using X-rays were performed as early as 1925 [47]. X-ray diffraction is categorized based on the energy and the shape of the beam. The two main categories leading to the present study are high-energy X-ray diffraction and micro-beam

X-rays diffraction giving high spatial resolution, also known as the micro-diffraction technique. Recent advances include the use of high-energy X-rays (with more penetrating power) and micro-diffraction with sampling volumes of a few μm^3. Both of these are best performed at synchrotron facilities, and a combination of which are necessary for a comprehensive study.

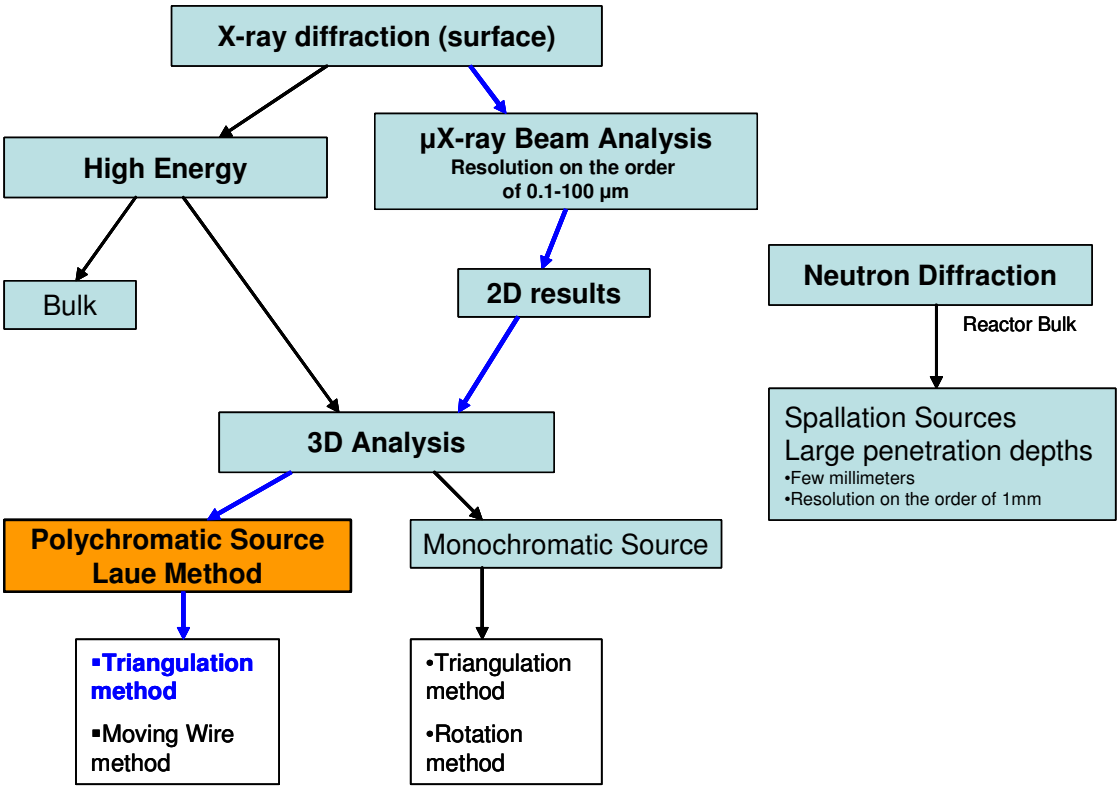

Figure 1 Classification of Radiographic Techniques (Dates are taken for first publication in literature).

High-energy X-rays were first utilized for bulk studies wherein the macro effects of the composite constituents were studied simultaneously considering the matrix and many reinforcements as a bulk.

Using highly spatially-resolved beams which now approach the nano-scale (10 μm-100 nm) in size, sub-grain analysis can be made where in the individual grain behavior is studied. This is a new technique (2002) due to the continuing development of the focusing optics and other precision equipments involved. This category of X-ray studies can further be applied to 2D and 3D studies of materials.

The three dimensional analysis involves specially developed techniques such as the triangulation method [48] and the moving wire method [49]. These however, are applicable with the use of polychromatic X-ray sources. Experiments conducted using monochromatic X-ray sources utilize a rotation and a similar triangulation method for obtaining 3D data.

Before High-energy XRD, Neutron diffraction measurements were utilized, where the materials were dense and required deeper penetration for their analysis. Due to flux limitations, the resolution on Neutron diffraction experiments is restricted compared to that of the X-ray diffraction techniques. Neutron diffraction is generally applied to bulk studies.

X-rays can effectively be used to study the material structure and internal properties. A further study of the crystal structure shows that data such as strains and stresses within a material can also be observed. The use of diffraction methods for measuring the stress involves the use of inter-planar spacings. The crystal of the constituent material itself acts like a strain gauge. The technique can thus be used to find internal residual stresses

and also the material's response to an externally applied load. Like visible light, X-rays are subject to diffraction when they travel through appropriate media and behave in accordance with the Bragg's Law. The concept is used for the analysis of the composite used in the current experiment. The aluminum matrix, which is polycrystalline in nature, when deformed elastically, using external loading, the lattice plane spacings in the grains change from the stress free dimension to a strained dimension in proportion to the applied loading. This change in lattice plane spacing is observed using the principles of diffraction with the help of high-energy synchrotron X-rays. The grains act as diffracting surfaces for the incident X-ray beams.

3.1 Bragg's Law of Diffraction

Diffraction of electromagnetic waves or light in general is governed by the basic law called Bragg's law. Bragg's law relates the diffraction angle (θ), the inter-planar lattice spacing (d), and the wavelength of incident light (λ). Consider, the wave front or wave plane to be incident on a set of atoms which are arranged along two planes A and B. The vector X_1 is a unit vector which represents the incident beam and the vector X_2 is one in the direction of the departing wave-front which is also the diffracted portion of the wave. As shown in the figure, the wave-front is diffracted at two different points namely point 1 and 2. The angle of incidence is θ; and, since there exists symmetry about the normal in diffraction, the diffracted portion exits at angle θ also. The final difference between the exiting portion of the wave-front and the incident wave front is $(X_2 - X_1)$. This difference is normal to the diffracting planes.

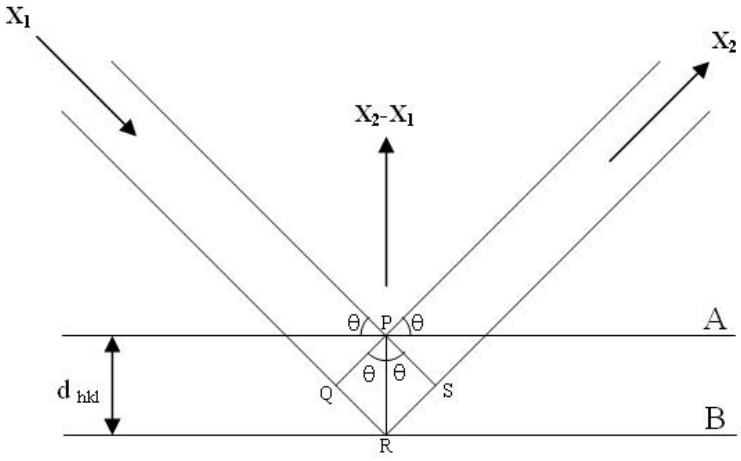

Figure 2 Schematic of the Diffracting planes on which the incident beam is diffracted

The points P, Q, R and S are seen to define two triangles with base angles equal to θ. Using geometry and considering the two triangles PQR and PRS,

$sin\theta = \frac{QR}{d_{hkl}}$ and $sin\theta = \frac{RS}{d_{hkl}}$,

Hence $QR = RS = d_{hkl} \sin\theta$. (3.1)

Considering constructive interference of the two wave fronts, in which the diffracted wave fronts from P and R are in phase, then $QR + RS = n\lambda$. (3.2)

Using the equation 3.1 and 3.2,

$$n\lambda = 2d_{hkl} \sin\theta \quad (3.3)$$

Equation 3.3 depicts the Bragg's Law in which *n* is an integer used by convention. Bragg's Law relates the wavelength of the incident beam, the angle of incidence and the inter-planar spacing.

For the composite under consideration, consisting of two different kinds of materials, namely the polycrystalline face centered cubic Aluminum alloy (A356) and the rhombohedral Sapphire single crystal (Al_2O_3), there exist two different values of d_{hkl} . The inter-planar spacing is a value of the normal distance between a set of parallel planes of a crystal. The planes with large spacings have low indices, and intersect a large number of lattice points [21]. The inter-planar spacing d_{hkl}, measured at right angles to the planes is a function of the miller or plane indices (*hkl*) and the lattice parameters ($a,b,c,\alpha,\beta,\gamma$). Hence there exist different values of the *d* spacing for the matrix and the fiber.

The inter-planar spacing for an unstrained crystal based on the Miller indices and the lattice parameters are shown below. The following equations present the suitable equations for cubic crystals and rhombohedral crystals.

Cubic

$$d_{hkl} = \frac{a_o}{\left(h^2 + k^2 + l^2\right)^{1/2}} \tag{3.4a}$$

Rhombohedral

$$\frac{1}{d_{hkl}^2} = \frac{\left(h^2 + k^2 + l^2\right)\sin^2\alpha + 2\left(hk + kl + hl\right)\left(\cos^2\alpha - \cos\alpha\right)}{a^2\left(1 - 3\cos^2\alpha + 2\cos^3\alpha\right)} \tag{3.4b}$$

The abovementioned equations hold true for pure crystals and hence are utilized in calculating the inter-planar spacings of perfect crystals.

Considering the fundamental equation of strain (ε) which by definition is the ratio of the change in the length to the original length,

$$\varepsilon = \frac{\Delta l}{l} \tag{3.5}$$

The change in length is analogous to the change in the inter-planar spacing within the deformed crystal lattice. The original length being the *d*-spacing of the perfect crystal. Hence,

$$\varepsilon = \frac{d - d_o}{d_o} \tag{3.6}$$

Thus the total strain in a particular deformed crystal can be obtained.

In terms of crystallographic analysis of materials, a *grain* is termed as a collection of crystal lattices with unique orientation. A grain which is lined up at a specific crystallographic orientation which satisfies the Bragg condition diffracts the incident X-ray beam. Thus diffraction spots are obtained from specific grains which are oriented at a particular Bragg angle θ.

The Bragg angle is dependent on the wavelength of the incident radiation as seen in equation 4.3. Thus, when an X-ray beam of a particular wavelength is incident, only those grains, which are aligned at the corresponding Bragg angle, produce a diffracted image on the CCD. The polycrystalline Aluminum A356 matrix in the composite consists of grains which are distributed at random orientations with respect to the incident beam. To cater to this fact, the experimental procedure uses a focused polychromatic X-ray beam (also called white beam) which consists of a range of wavelengths. This facilitates

collection of diffraction data from a large number of grains as opposed to the use of a monochromatic X-ray beam which would select for diffraction only those few grains where were aligned to the particular θ (the difference is 2 orders of magnitude).

Application of X-ray strain measurements requires extreme care, especially when considering the level of accuracy required measuring strains.[1] In the general case when stress is applied to a polycrystalline material or composite, the total strain measured with diffraction at any point includes three terms [50]

$$\varepsilon_{ij}^{total} = \varepsilon_{ij}^{o} + \varepsilon_{ij}^{inter.} + \varepsilon_{ij}^{res.} \tag{3.7}$$

where, ε_{ij}^{o} is the homogeneous elastic strain due to applied stress σ^{o} (if the material were a homogeneous isotropic body), $\varepsilon_{ij}^{inter.}$ is the interaction (or coupling) strain due to elastic incompatibility or inhomogeneous plastic yielding, and $\varepsilon_{ij}^{res.}$ is residual strain. Each of these terms is an average value over the sampling volume, which depending on the choice of radiation may involve only a few grains or even a sub-grain region.

[1]Many materials yield or fracture before the elastic strain reaches 1% (typically (0.2% to 0.5%).

CHAPTER 4

4.0 LAUE DIFFRACTION

4.1 History of Laue Diffraction

Laue diffraction discovered by Max Von Laue was developed almost parallel with Roentgen's discovery when P.P. Ewald discussed his doctoral thesis on optical properties of crystals with Laue, which led to Laue's proposition that crystals lattices illuminated with wavelengths of the magnitude equal to that of the atomic spacing would act as resonators which could lead to some kind of diffraction effects. [51] To confirm the proposition, first experiments were conducted on a crystal of copper sulfate in coordination with Friedrich and Paul Knipping [51]. The photographs taken with the beam irradiating different portions of the same crystal gave constant results. The photographs showed up spots for the crystal illuminated.

Historically Laue diffraction was used solely for the purpose of determination of crystal symmetry and cell dimensions. The method still had some intrinsic limitations which showed up when applied to crystal-structure determination which was due to the fact that the exact wavelengths and intensity of the incident wavelengths could not be specified. This greatly restricted use of Laue diffraction method to the determination of crystal orientation and perfection.

The development of sophisticated optics and focusing technologies, along with powerful synchrotron sources with finer beam sizes, has lead to the rediscovery of Laue diffraction. These developments not only provide beam sizes on the meso-scale, but help specify a precise wavelength and intensity of the incident radiation.[66] Furthermore, powerful radiation sources with polychromatic as well as monochromatic nature available at microscopic beam sizes can now illuminate samples and data can be collected instantaneously using fast charge coupled area detectors. Previously, this had to be done using photographic plates which were time consuming and cumbersome to use.[51] Moreover each spot obtained on the photographic plate had to be manually indexed and analyzed based on manual measurements of the positions of the spots. The overall technological advances, including the computing capabilities now enable the use of the Laue method.

4.2 Laue Diffraction Method

Laue diffraction is based on the diffraction laws proposed by Bragg and utilizes Bragg's equations for the calculation of the strains within the sample. The mathematical steps mentioned in the preceding section explained the calculation of the strains from the *d*-spacings which are obtained from diffraction spots recorded onto a CCD. These spots exist in a specific manner on the CCD, which are specific for a particular material and are called *Laue Spots*. The specimen being studied is placed in a 90º Laue diffraction geometry. Extraction of useful data such as the *d*-spacing from these Laue spots is important. Each portion of the white diffracted beam in the Laue method has a different

wavelength, and depends on the value of θ and d of the crystal plane producing the reflection.

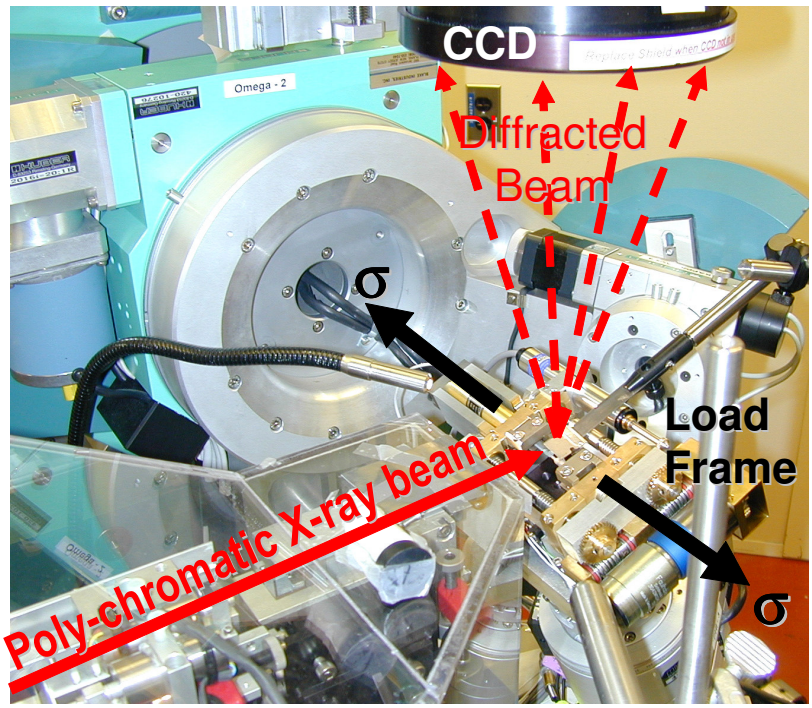

Figure 3 Photograph of experimental setup showing path of the polychromatic X-ray beam, the composite sample held in the load frame, and the paths of the diffracted beams being projected onto the CCD.

Figure 3 depicts the way in which the composite sample was placed on the experimental setup. This is a 90º reflection geometry wherein the charged couple detector is placed at a right angle to the incident white X-ray beam. The incident beam is focused using the focusing optics and made incident onto the composite sample placed on the precision translation stage. The diffracted spots from the matrix and the fiber are incident on the CCD. Typical images showing the Laue spots in the case of the Aluminum grains and the Sapphire crystal are shown in Figure 4.

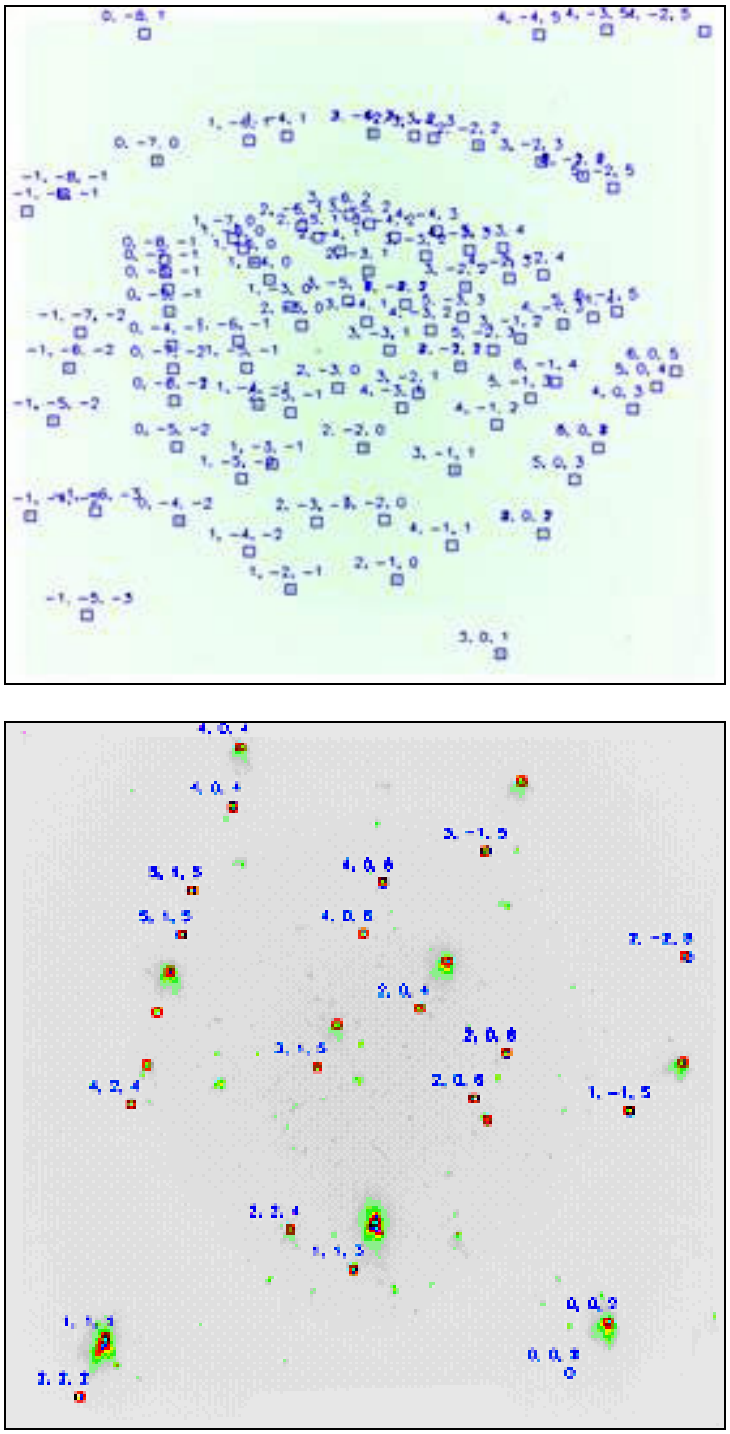

Figure 4 (Top) Indexed using XMAS Laue patterns of the rhombohedral sapphire crystal (fiber). (Bottom) Indexed Laue patterns of the Cubic Aluminum (matrix).

The spots seen Figure 4 represent the reciprocal lattices in reciprocal space. The "Reciprocal Lattice" is so called because the properties of such a lattice are reciprocal in nature to the ones in real space.

A typical lattice in reciprocal space satisfies the following properties.

- A vector H_{hkl} drawn from the origin of the reciprocal lattice to any point in it having coordinates *hkl* is perpendicular to the plane in the crystal lattice with Miller parameters *hkl* and is given in terms of its coordinates in the form of the expression

$$H_{hkl} = hb_1 + kb_2 + lb_3 \tag{4.1}$$

  where b_1, b_2 and b_3 are the vectors defining the reciprocal lattice.

- The length of the vector H_{hkl} is equal to the reciprocal of the spacing *d* of the (*hkl*) planes,

$$H_{hkl} = \frac{1}{d_{hkl}} \tag{4.2}$$

Each reciprocal lattice point is related to a set of planes in the crystal and represents the orientation and spacing of those set of planes.

The analysis of the Laue spots to extract valuable information requires an understanding of the way the spots are arranged onto the CCD. Numerous approaches have been developed to analyze the spots to obtain information regarding the lattice parameters [21, 52].

4.3 Application of Laue X-ray Diffraction

The ability of high energy X-rays to penetrate deep within the materials supports non-destructive material studies. The method provides us with the ability to actually measure the strains and stresses within the constituent grains of a material which cannot be realized without the use of such techniques. The experimental procedure also helps in corroborating previous theoretical efforts in this direction [37,33,71]. The final results are brought out in the form of the measured residual stresses that exist in an aluminum sapphire metal matrix model composite which was considered in this case. The composite is further subjected to external tensile loading and corresponding effects at the loads are presented. An important fact that arises in the experiment is the advantage of existing compressive residual strains within the matrix upon loading in tension along the axial direction. The determination of strains from experiments utilizing Laue diffraction requires precise indexing of every grain and determination of the exact orientation and position data. The accuracy of the final strain data relies on how accurately the Laue spots are indexed. Hence, an effective method to extract data has been sought after. The complexity in data interpretation of the experimental results had restricted use of Laue X-ray diffraction methods for measurements pertaining to single crystals [53,54] until the development of precise focusing equipments and computing environments.

Extensive work related to the automated indexing of the diffraction spots has been carried by J. S. Chung et al.[55]. As experimented earlier by Young-Han Park et al. [63], the Laue reflection geometry is usually the standard method utilized to determine crystal data without rotation of the sample. The diffraction spots from an illuminated sample volume

are indexed using the code by Chung et al. following a systematic flowchart that was used in their procedure. The flowchart utilized is as shown in Figure 5. The flow chart describes a step by step procedure from Laue pattern measurement to the grain orientation determination followed by the determination of either the deviatoric or absolute strain tensor.

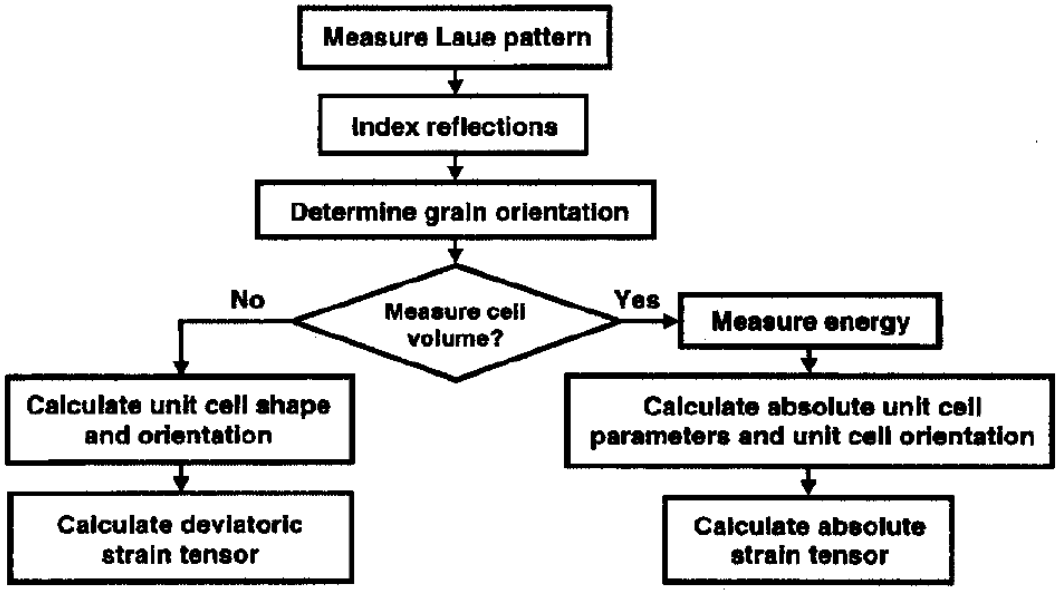

Figure 5 Flowchart of steps implemented in the indexing code [55]

The above procedure proceeds with explanation of the development of a strain tensor for a unit cell, followed by the determination of unit cell parameters and finally explanation on the indexing technique is given. This technique proves to be advantageous since the code implemented is effective in correctly indexing the spots based on a very few number of reflections unlike prior techniques described earlier by I. A. Shermetyev et al.[56], R.B.G. Ravelli et al.[57] and H.R, Wenk et al.[58]. The procedure uses energies of each reflection for the determination of the lattice parameters. This is accomplished by

scanning the energy of the incident beam while Bragg reflections are monitored on the area detector. This is backed up by the fact that even though the two differently oriented crystals produce same Laue spots, the individual energies of respective reflections are different.

The code developed by Chung et al.[55] has been further developed and implemented for indexing data obtained from sub-micron X-ray diffraction by A.A. MacDowell [59]. This experimental work is comparatively recent and utilizes the much developed high-energy synchrotron radiation with high spatial resolution. The beam size is on the micron scale and is similar to the one used in the current research work. Also described is the newly enhanced version of the indexing code called XMAS (X-ray micro-diffraction analysis software). The technique utilizes an aluminum substrate covered with a silicon dioxide insulating layer as the sample. Diffraction spots are obtained from the diffracting aluminum grains which lie beneath the insulation layer, thus illustrating the sub-micron diffraction concept. The procedure is capable of measuring the strain values in Aluminum interconnects in electronic circuits with an accuracy of 0.01º in orientation and $2x10^{-4}$ of strain.

Experimental work on sub-micron X-ray diffraction [59] has further been extended by N. Tamura et al. [60]. Herein, the aspects of applicability of the above developed procedure for practical applications such as aluminum thin films, the study of the spontaneous growth of tin whiskers in lead-free solder finish and the measurement of strain fields around thin film buckling are considered. The experiment utilizes samples with minimal

thicknesses of the order of 1 to 2μm for the analysis and depth of penetration of the beam is at smaller scales.

Experimental evaluations of the above have been conducted to provide analytical parameters such as flow stress, strain distribution, in particular the change with change in applied loads, orientation data and, most recently available, is the inter-granular stress parameter. Also possible, is the measurement of data related to grain boundaries using a newly developed technique by Wenjun Liu et al. [61]. The procedure utilizes a monochromatic or a polychromatic light source to illuminate a particular sample volume. The experimental setup used is shown below.

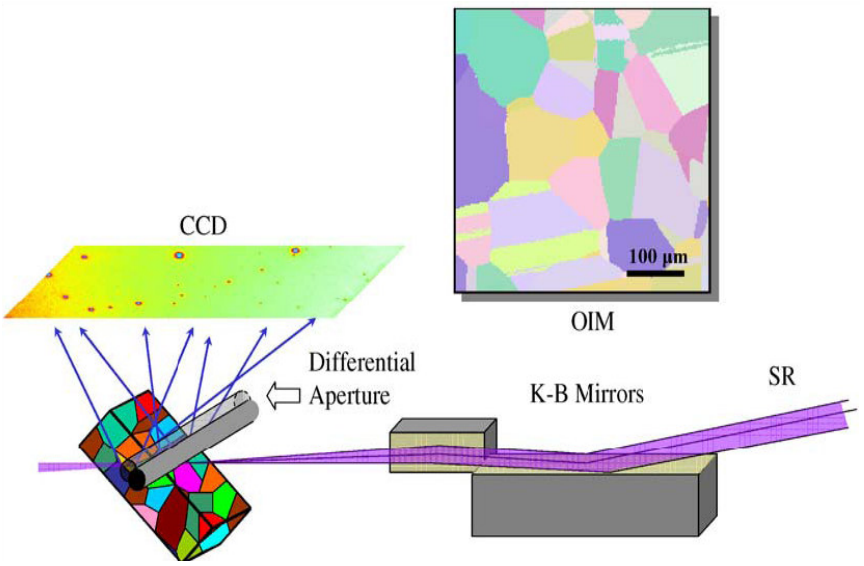

Figure 6 Experimental setup of the 3-D grain boundary classification using Pt. Wires [61]

Using a moving aperture created by a moving platinum wire, a differential scan of diffraction spots is done. The research provides a method to experimentally determine the grain boundary networks within the polycrystalline materials. It provides initial results in

a direction which would lead to analytical explanation of the deviation of grain boundary structures from the coincident lattice site models.

4.4 Experimental Work on Behavior of Poly-Crystals.

Preliminary work has been done regarding the development of strain tensors for single grains among the polycrystalline bulk by L. Margulies et al.[62]. They outline the development of the strain tensors using measurements performed by the rotation method, and using automated indexing routines to group reflections belonging to a single grain. The automated code used is based on the Lorentzian fit to index individual diffraction spots to a particular lattice structure. The above mentioned procedure was utilized for strain measurement on a particular individual grain. The technique was successful in determining only three strain components out of the whole strain tensor. The procedure is restricted to a single grain with precise alignment of the grain with the incident beam due to occurrences of large errors in the strain readings when the sample is rotated.

Initial developments related to the 90º Side-Reflection Laue Technique were carried out by Young-Han Park et al. [63] and also by A. L. Patterson [64]. Their work provides key initial developments in the field of Laue diffraction for strain analysis. The experimental procedure successfully utilized the 90º reflection geometry for diffraction analysis which was possible due to simultaneous advances in synchrotron sources and computing environments. However, the study is only successful in bringing up the preliminary procedures with no statistical results.

J. Böhm et al. [65] have conducted experiments on Internal stress measurements by high-energy synchrotron X-ray diffraction at increased specimen-detector distance. Their procedure involves illuminating a sample volume with high energy monochromatic X-ray radiation to produce diffraction rings. Every diffraction ring is then recorded on a large area detector and deviation of diffraction rings from their original position is analyzed to extract strain information. Since deviations in the ring positions are minute the procedure demands for the use of a large detector to sample distance which in their case is about 7m. Example diffraction rings obtained from such a procedure are shown in the figure below.

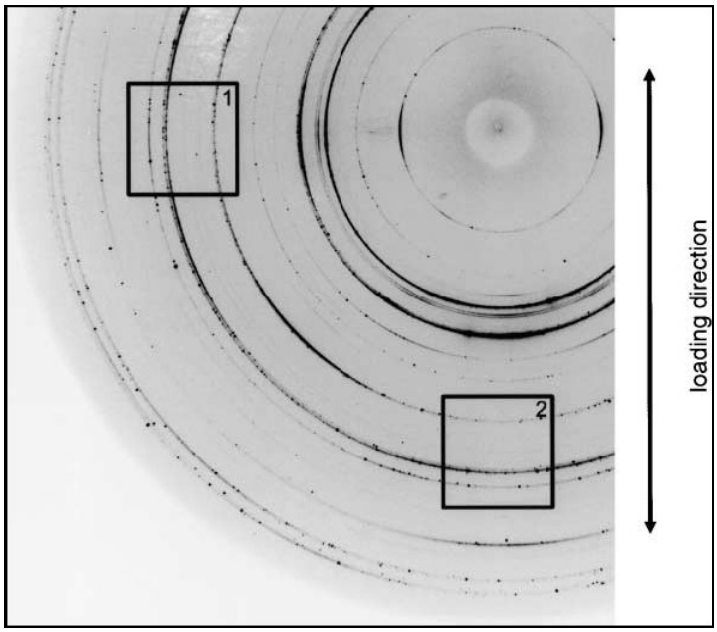

Figure 7 Diffraction pattern of the γ-TiAl-based [65]

Also, shown in Figure 8 are the analyzed areas which show displacement of the rings from their original position. The strains are analyzed using the $\sin^2\varphi$ method of strain calculation which is one of the method used to analyze 2-D data from image plates or area detectors[6, 21].

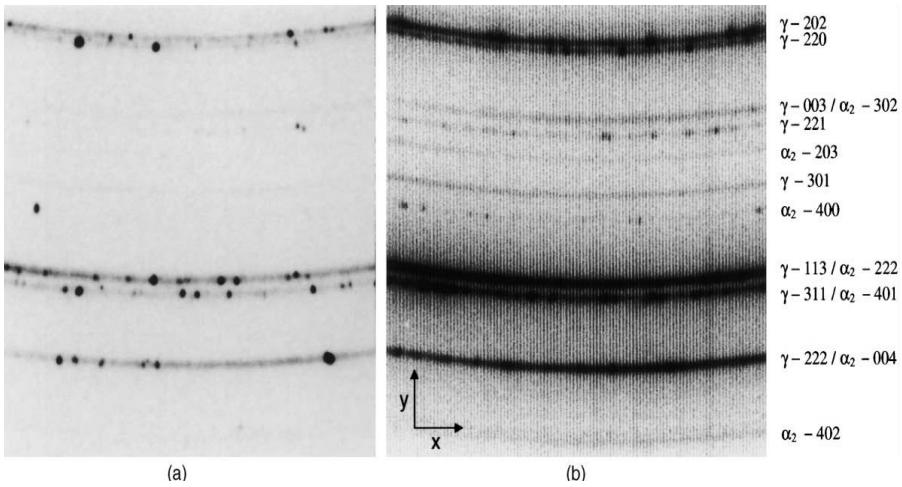

Figure 8 Enlarged portions of area 1 are shown in (a) & (b) which are indexed to respective planes [65].The two images were obtained two different kind of area detectors.

This experiment however can be used successfully in case of polycrystalline materials. Using it for analyzing single crystalline material is difficult due to diffraction as spots instead of rings. The experimental output of such a material is hard to analyze due to accuracy of measuring a few spots. Another disadvantage of using such a technique is the loss of crucial data in the unrecorded part of inverse space (other unrecorded spots). To overcome this problem a larger detector would be necessary which is not feasible.

CHAPTER 5

5.0 METHOD

As elaborated in the previous sections, there has been an ever increasing need to develop high performance materials, for which, understanding the underlying properties of materials at microscopic levels and beyond plays a crucial role. Most properties of materials rely on the structural characteristics at a meso-scopic level (0.1-10μm) which consists of the grain boundaries, dislocations, impurities, intra-granular, and inter-granular stress distributions, and also residual strain distributions. The task of understanding underlying properties of composites is difficult. Heterogeneous networks of second phases, randomly oriented grains, voids, reinforcing particles and fibers act to redistribute macroscopic applied loads into complex three-dimensional distributions of stresses and strains. [66]

Due to lack of knowledge of the material behavior at such scales, there has been limited work in modeling and theoretical developments which provide a supporting connection of material properties from the microscopic to macroscopic level. With the advent of technology in focusing optics, high energy X-ray generation and computing power, it has become possible to study materials at larger depths and at more refined scales. The

widely used technique of X-ray diffraction can now be used at a micron scale to measure the meso-scopic properties. Once projected onto a sample of interest, the diffracted X-ray micro beam (if poly-chromatic) generates an ordered pattern of diffraction spots which contain information on strain. The pattern of the spots produced is unique for a particular kind of crystal structure. Hence, using the known pattern from an unstrained crystal which is similar to the constituent crystal structure the existing strains in the sample are determined.

It naturally follows that a study on a practical high-performance MMC would be of significant value to the modeling and eventually engineering community. One such composite is the Al-matrix/Al_2O_3-fiber composite. Both Al and Al_2O_3 are well known as structural materials. Naturally, the Al-Al_2O_3 composite itself has received considerable attention from other researchers simply due to the performance characteristics of its constituents [31, 32, 67, 68]. However, the fundamental lack of phase-specific micromechanical data remains. The key objective of the current experimental procedure is to determine the strain distribution in a polycrystalline material sample at a microscopic level. Since material behavior no longer remains the same in the case of composites as compared to the individual material [43,46], the characteristic effects in case of a typical fiber reinforced composite are studied under conditions of loading.

The composite used for the experimental evaluation consists of a matrix of Aluminum (A356) alloy reinforced with single crystal sapphire (Al_2O_3) fiber. The sample consists of a single fiber within the matrix. Such a sample was used because it serves as a model

3D composite with the necessary characteristics to observe strain behavior within a composite. Another important reason behind using such a small sample was time reduction in the measurements and limitations of the depth of penetration. Synchrotron X-rays were required to obtain the necessary intensity to reduce the beam size below the fiber diameter which in the present case is 140μm across, while maintaining sufficient diffraction statistics and strain resolution over reasonable count times. The technique described may be tailored for specific mechanical information and is applicable to a variety of composites. Scales from the sub-micro (0.5 μm) to micro (several μm) are simultaneously available with this method.

Since the two materials used in the composite have different coefficients of thermal expansion and also different stiffnesses, the composite is expected to have pre-existing macroscopic residual strains prior to loading. In addition, the anisotropy of the aluminum grains contributes to residual strains at the micro scale. The experiment aims to reveal how the residual strains are distributed throughout the composite and within certain assumptions will also be able to give actual values of the strains. Another goal is to determine the strain distribution in the highly stiff fiber and the interaction of the polycrystalline matrix with the fiber. A new technique recently developed to find and calibrate the absolute strain values using Bragg-edge diffraction is described and tested for the first time on a fiber composite. The strain distributions in individual grains in the matrix are determined using an average of results over the entire grain. The technique is effectively implemented to differentiate each existing grain in the field of view and also determine its position with respect to the incident X-ray beam in 2D. Once the strains

from the observation field have been mapped, the images of the polycrystalline matrix and the single crystal fiber are superimposed to obtain a comprehensive view of the composite being studied.

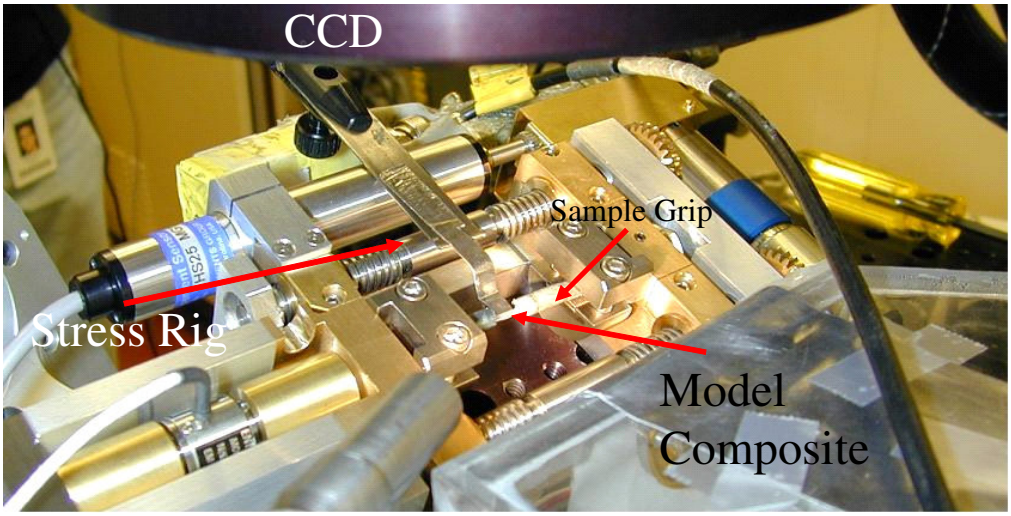

Figure 9 Photograph of model composite sample mounted in the adapted stress rig. Also seen is the CCD above in a 90° reflection geometry. Sample width: 0.6 mm.

Figure 9 shows a photograph of the sample mounted on the adapted Fullam SEM stress rig which along with the sample is mounted onto the translator stage on the goniometer. The CCD is placed vertically above the sample and is at a right angle to the incident X-ray beam. In this orientation, the open face of the load frame allows X-rays to reflect from the surface of the sample.

5.1 Approach

The following introduces the use of the special technique of micro-Laue X-ray diffraction to measure strain. Some issues concerning the application of stress to a diffracting body are also presented. This technique is substantially different from monochromatic X-ray

diffraction methods. Since the detection of the strains within the deeply lying grains within the sample has been the main focus, the primary requirement for the X-ray diffraction analysis is the use of high-energy X-ray source with high spatial resolution. The experiment was conducted at Beamline 7.3.3 at the Advanced Light Source, Berkeley (ALS) (1.9GeV, 1.27 T, 400 mA) by Dr. Jay C. Hanan and Dr. Nobumichi Tamura in October 2001. Unlike the majority of X-ray diffraction analysis experiments, which involve monochromatic incident beams, the current experiment utilizes a polychromatic X-ray beam which typically consists of a wide range of wavelengths (2kev to 14keV). The main advantage of using the latter in this case is to obtain diffraction spots from a larger number of grains.

5.2 Sample Preparation

The model composite sample was prepared by Dr. Jay Hanan by quenching the A356 aluminum alloy from 700^{o}C around the single crystal fiber. During the quench, the fiber was held in place by slits at each end of a graphite mold. In order to dry the mold and reduce the thermal shock to the fiber, the mold was also heated to 700 ^{o}C. The molten aluminum alloy was poured into the hot mold. The alloy was allowed to surround the fiber prior to the final quench in room temperature water.

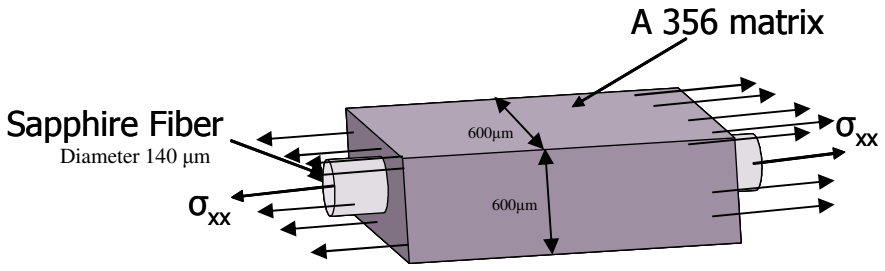

Figure 10 Model composite consisting of the aluminum A356 matrix and sapphire fiber within. Load was applied axially as shown.

This process can lead to void formation in the matrix. Finally, the sample was resized using EDM, leaving the fiber at the center of a 600 µm square.

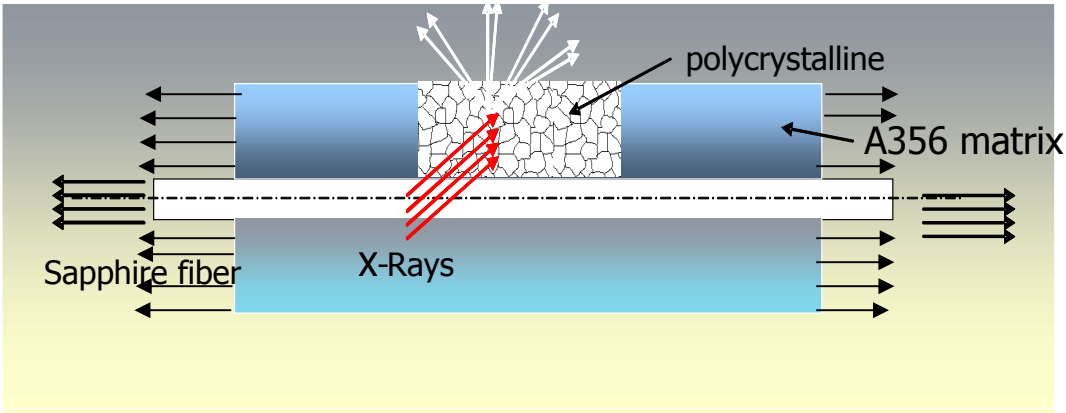

Figure 11 Cross sectional view of the Aluminum matrix (polycrystalline) and sapphire single crystal. X rays are seen diffracting from the matrix(The above figure is a sketch, not the actual model composite).

The above shown model composite was held in specially made grips using high strength glue. These grips were further clamped into knife edge grips of the stress rig. This is shown in the Figure 12. Such a method to grip the sample is required to avoid possible damage of the Sapphire fiber, due to crushing which leads to failure of the composite at the region where it is gripped. Also the low profile grips minimize shadowing of the diffracted beam.

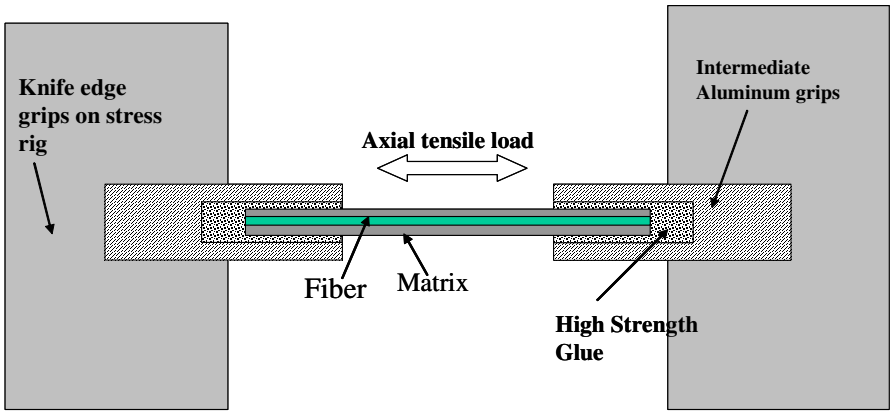

Figure 12 Schematic showing the sample held in the grips. Note the large knife edge grips in comparison to the aluminum intermediate grips. The large grips cause shadowing of the diffracted beam when placed close to the sample.

5.3 The Experimental Setup

With X-ray diffraction's ability to measure strain, it follows to apply the analysis to a body under applied stress. Mechanical loading is not new to XRD. Even though a large number of experiments have been carried out using X-rays for strain measurement, advances in focusing optics and computing power enhances the measurements to a higher degree. The first mechanical loading experiments on unidirectional MMC composites performed recently by Hanan et. al. [69] using diffraction with simultaneous tomography took advantage of their custom load frame designed for simultaneous diffraction and imaging. The combination of diffraction and imaging is a newly developed technique which will result in further progress in our understanding of composites. Since imaging was not performed for the present study, an adapted Scanning Electron Microscope (SEM) load frame designed by Fullam,[2] was used for this study (see Figure 9).

[2]Ernest Fullam Inc., 900 Albany Shaker Rd., Latham, NY 12110-1491.

Measurement of residual strains is done at no applied load and is done by carrying out the regular beam scans on the sample initially. To understand effects of applied load on present residual stresses and hence the composite, the sample is subjected to successive load steps. In order to track the load on a sample mounted in an X-ray goniometer, a program was designed in LabVIEW[3] 6i. The load cell used was an Entran[4] ELHS-T1M-1KL which requires a 10 to 15 V excitation to measure forces up to 6500 N. The output voltage from the load cell is proportional to the applied load on the sample. Using digitization hardware, the output voltage can be read by a computer using the LabVIEW program. The time corresponding to the load cell reading by the computer is correlated with the start and end time of the diffraction measrurment. [3]

To induce controlled stresses in the composite, the sample was gripped into the stress rig using EDMed adapters reinforced with epoxy. The stress rig mounts onto a precision three axis stage. The whole setup is arranged in reflection geometry, as shown in Figure 13 wherein the detector is placed at a right angle to the incident beam. The incident beam is diffracted by the many grains it encounters and creates diffraction spots on a charge coupled detector (CCD). The polychromatic X-ray beam from a bend magnet is focused to a size of 700 x 800 nm^2 using a pair of elliptically bent Kirkpatrick-Baez mirrors.

---

[3]The LabVIEW software is commercially available from National Instruments, 11500 N Mopac Expwy, Austin, TX 78759-3504.

[4]Entran Devices, Inc. 10 Washington Ave., Fairfield, NJ 07004-3877.

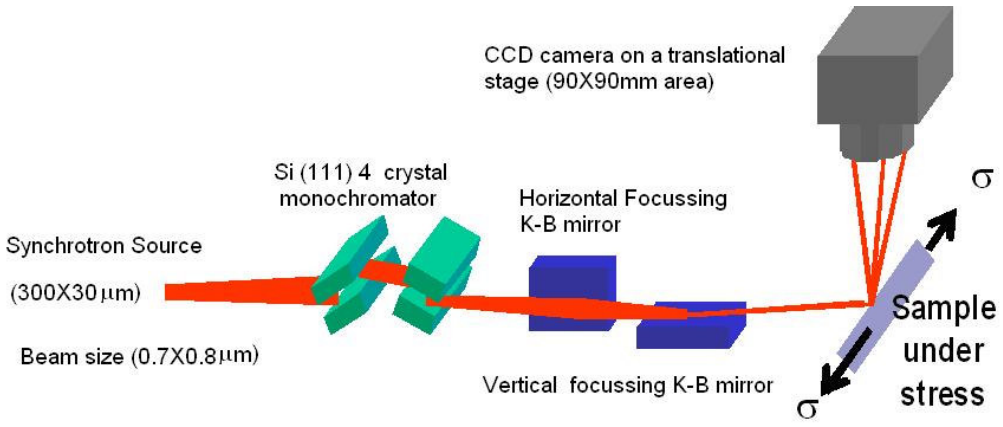

Figure 13 Diagram of experimental setup at ALS

The sample is scanned under the resulting submicron X-ray beam over a rectangular area of 0.3 mm x 0.5 mm at a step size of 10 μm forming a grid of 34 x 51 data points. At each step, the Laue pattern generated by the X-ray illuminated volume of the sample is collected using a Bruker SMART 6000 X-ray CCD detector.

The data obtained from the CCD is in the form of images consisting of ordered spots. The composite gripped in the load frame was mounted onto the high precision translation stage which facilitates in moving the sample in the X and Y directions of the laboratory coordinates. Since it is not possible to move the X-ray optics and the whole experimental setup in order to scan the whole surface of the composite, moving the sample itself is moved using the translator stage. The sample was moved on a set of stages which reliably move in 10 micron steps, and the field of view on the composite under consideration, was scanned at intervals or "grid points." For the first measurement at no applied stress, the whole scan consists of a grid of 34 x 26 points over the area when the sample was not loaded. To increase the resolution the spacing was reduced in the axial

direction and the grid was of 32 x 51 points across for the measurements at applied stress. Hence there are 34 x 26 diffraction images which when resolved and analyzed would give a residual strain distribution along the sample. The beam size used to map the strains had a dimension of 0.7µm X 0.8µm. The type of grid in which the points are scattered is shown in Figure 14.

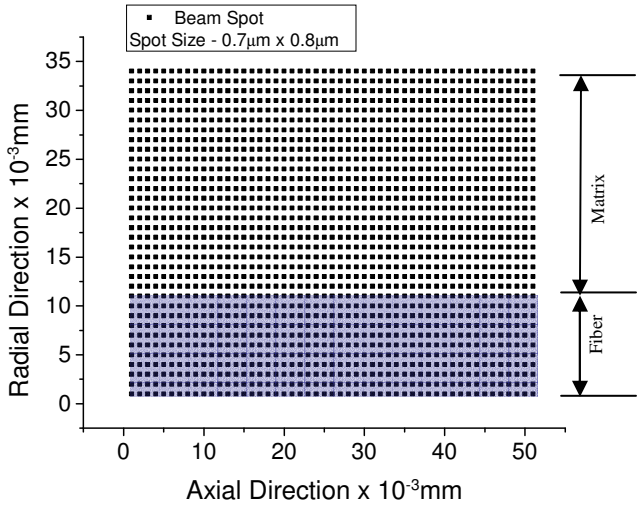

Figure 14 Grid of data points across the composite sample at a stress of 80MPa.

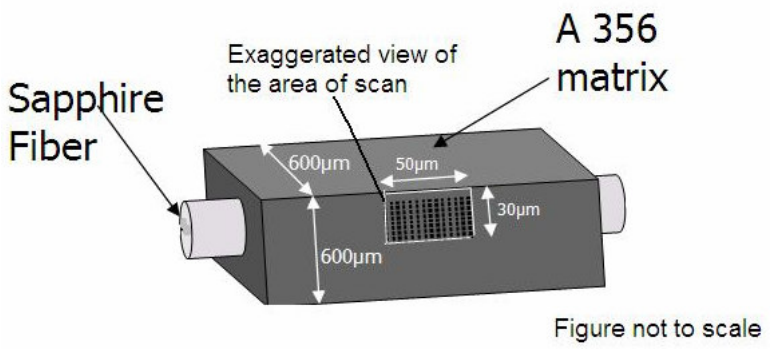

Figure 15 Illustration of the location of the grid of scanned points

Each dark point represents the position on the composite where the beam was incident. Each grid point is spaced at 10µm apart. These points represent the position in the XY

plane, which consists of the axial direction along the abscissa and the radial direction along the ordinate, at which the diffraction spots are obtained. Upon resolving the strain data for each point, a strain contour map may be plotted. This plot shows the grains that lie across the area. Although a whole strain tensor is available, for the current analysis, the strain in the axial direction ε_{xx} was primarily considered.

For determination of the nature and behavior of the composite under tensile loading, the experiment was carried out in three load steps. The first sets of measurements were made at no applied load. Subsequent measurements were made at loads of 80 MPa and 120 MPa. The measurements at no load condition will help determine the presence and degree to which residual strains exists. This measurement reveals the actual values and nature of strains that exist namely compressive and tensile.

As explained in chapter 4 the ability to procure accurate quantitative information related to orientation and strain/stress tensor is important. This particularly requires an extensive computer code which is automated and can index the spot patterns obtained from the CCD at a fast rate.

5.4 Indexing Software – Analysis method

In the current case, indexing was carried out using a code called XMAS (X-ray micro diffraction analysis software) which was developed at the Advanced Light Source. The code is based on a previous platform developed by Chung & Ice (1999)[55]. A detailed explanation has been described by Tamura et. al. [70] and briefly discussed below. Once

the beam is made incident onto the sample, which produces diffraction spots on the CCD, the acquired images are corrected for image intensity and spatial distortion. The next succeeding step is to find out the local peak maxima in the entire field of the CCD image. This is carried out by classifying the peaks according to their integrated intensity and finally fitting them using a 2D Lorentzian function. The use of this function allows the instrument to achieve sub-pixel resolution on the position of the peaks. The accuracy with which the peaks positions are fitted is one of the limiting factors for the strain accuracy that is measured. Upon finding out the peak positions the pattern of spots is indexed with the *hkl* Miller indices.

For carrying out the indexing, an iterative selection of the most intense peaks is done. This forms a subset of N most intense reflections. Using the scattering direction obtained from the instrument calibration procedure, a tabulated experimental list consisting of angular information related to $[N(N-1)/2]$ items is created and compared with the reference list of angular information from theoretical scattering vectors.

Matching triplets of reflections within a specified angular tolerance are determined, and each of the triplet information along with the corresponding (hkl) indices is used to calculate the initial trial orientation matrix. For a good peak fit and index, it has been found through experimentation that a minimum of twelve reflections are ideal. Hence the above procedure identifies individual grains based on the crystallographic orientation. Finally, after calculating the positions of the reflections on the CCD, and knowing the

exact position of the CCD with respect to the incoming beam, the respective Bragg angle θ can be calculated.

5.5 Calculation of the Whole Strain Tensor

There exist five independent parameters which play an important role in the calculation of the strain tensor. These are the X and Y coordinates of the centre channel on the detector, the distance from the channel to the point of incidence on the sample and two angular parameters describing the angular information of the CCD also known as the tilt angles. A method of non-linear least-squares refinement technique is further used to calibrate these geometrical parameters [70]. Finally with the available calibrated fixed geometrical parameters and the variable lattice parameters *a, b, c, α, β,* and *γ*; the distorted unit cell parameters are calculated. These values obtained are used in calculating the whole strain tensor using strain equations explained in Chapter 4. Use of energy indiscriminate white beams allows observation of lattice distortions, not the overall change in volume (or dilatation). Hence only deviatoric strain components are observed from which the values of *a, b*, and, *c* are refined.

The strain tensor $\boldsymbol{t_{ij}}$ consists of both the rigid body rotation terms and the distortional components. However, the rotational component gets eliminated, because it is anti-symmetric. This is given by the equation as follows.

$$\varepsilon'_{ij} = (t_{ij} + t_{ji}) / 2 - I_{ij} \tag{5.1}$$

wherein, I_{ij} is the identity matrix.

The complete strain tensor which contains the deviatoric tensor (ε) and the dilatational component (Δ) is given by

$$\varepsilon_{ij} = \varepsilon'_{ij} + \Delta \tag{5.2}$$

and the dilatational component(Δ) is given by,

$$\Delta = \delta I_{ij}$$

where $\delta = (\varepsilon_{11} + \varepsilon_{22} + \varepsilon_{33})/3$.

Also, Since

$$\varepsilon'_{11} + \varepsilon'_{22} + \varepsilon'_{33} = 0 \tag{5.3}$$

The final deviatoric tensor consists of only five independent terms and the dilatational component being the single unknown δ. Hence in principle the full tensor (six-strain component terms) can be determined from a single white-beam diffraction image plus the knowledge of the absolute lattice value of a single reflection. Thus, the elastic stress tensor may also be derived knowing the values of anisotropic stiffness tensor C_{ijkl}.

Thus,

$$\sigma_{ij} = C_{ijkl}\varepsilon_{kl} \tag{5.4}$$

5.6 Calculation of the *d*-spacing for sapphire fiber:

In the current experimental procedure, a relatively new technique developed by Tamura et. al.[70] has been utilized to find the *d*-spacing or the inter-planar spacing of the single crystal aluminum fiber and the aluminum grains for the purpose of calibration. The calculation of the *d*-spacing for the single crystal sapphire fiber included an additional

technique to the above mentioned method. The sapphire crystal has its C-axis oriented along the axis of the fiber. The measurement of the *d*-spacing utilizes a method of scanning the white beam along the fiber and the use of a Silicon crystal to eliminate a particular wavelength out of the whole range of wavelengths within the white beam.

Unlike the conventional method of directly measuring the inter-planar spacing using the direct diffraction measurements from the crystal itself, this technique uses the relation of inter-planar spacing of the monochromator crystal, the wavelength eliminated at a particular angle and the *d*-spacing of the sapphire fiber at a particular orientation.

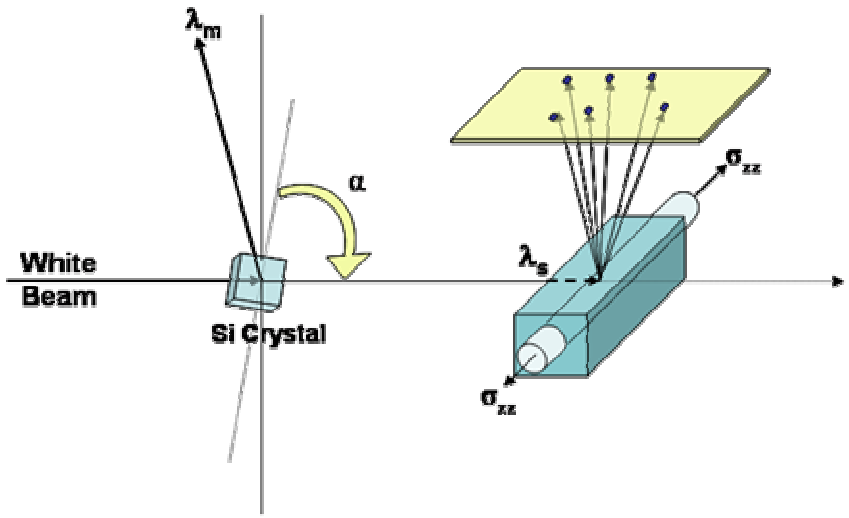

Figure 16 Silicon Crystal inserted in the beam. The Silicon crystal eliminates a particular wavelength out of the entire spectrum as a function of rotation angle α.

Figure 16 depicts the method of energy scans implemented for measurement of the *d*-spacing of the sapphire crystal. The Silicon crystal is oriented at a angle α with the incident beam. At the corresponding Bragg angle θ, the silicon crystal diffracts the

wavelength λ_m from the white beam. The rest of the beam is then incident onto the composite, with the sapphire fiber aligned in the beam path. The beam emerging out consists of all the wavelengths except λ_m. Using Bragg's equations, the initial diffracted portion of the beam is given by,

$$\lambda_m = 2d_{Si} \sin\theta \tag{5.5}$$

where θ can be chosen equal to α, the angle at which the crystal is aligned to the beam.

Hence, $\lambda_m = 2d_{Si} \sin\alpha$ (5.6)

At a specific value of α, a specific wavelength is eliminated. This value of α can be determined from a plot of the intensity of an individual Laue peak versus the tilt angle α of the Si crystal. At the desired value of α, the value of intensity suddenly drops as shown in the example plot of Figure 17.

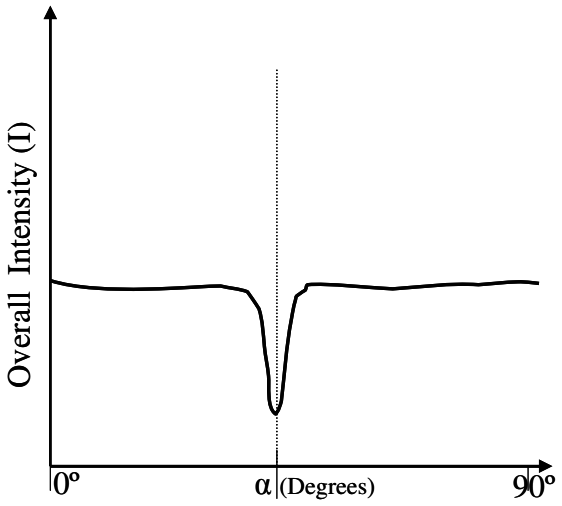

Figure 17 Variation of Intensity with change in Si Crystal angle as a function of rotation angle α.

There also exists a relation between λ_m and the d spacing related to the sapphire fiber given by,

$$\lambda_m = 2d_{sapphire} \sin\theta_{CCD}\,, \tag{5.7}$$

where θ_{CCD} is the Bragg angle for the selected diffraction spot on the CCD. Thus comparing the equations 5.6 and 5.7, a relation for the *d* spacing sapphire is obtained.

$$d_{sapphire} = \frac{2\sin\theta_{CCD}}{\lambda_m}$$

$$d_{sapphire} = \frac{\sin\theta_{CCD}}{d_{si}\sin\alpha} \tag{5.8}$$

Hence using the equation 5.8 the *d*-spacing for the sapphire crystal is effectively obtained. These values may also serve as calibration data when the strains are resolved for the polycrystalline matrix.

5.7 Selection of the Grain List for the Aluminum Matrix

As mentioned in section 5.2, the software code iteratively selects spots based on an integrated intensity and indexes them. The matrix consists of grains with a varied size distribution which makes larger grains to be indexed in multiple CCD images. This causes a grain to be re-listed many number of times by the software. Since the process of strain analysis is quite time consuming, the analysis is restricted to a few grains. Only 16 grains each with a specific orientation, which are prominent on the basis of occurrence are chosen. To implement this, the grain list is sorted in accordance to the frequency of occurrence and a Histogram is plotted which reveals the most prominent frequently occurring grains. Figure 18 shows the histogram plot which shows the grain numbers on the x-axis and Occurrence along the y-axis. The grains are listed by the software assigning each orientation a local index number. Each grain was separated based on crystallographic orientation and assigned a "grain number." Many of the "grains" are not

observed more than 30 times in the area of observation and have a small area. For the grains that have a large area (>120 observations = 110μm across) the morphology, orientation, and relative strain was sufficient to identify individual grains at each applied stress.

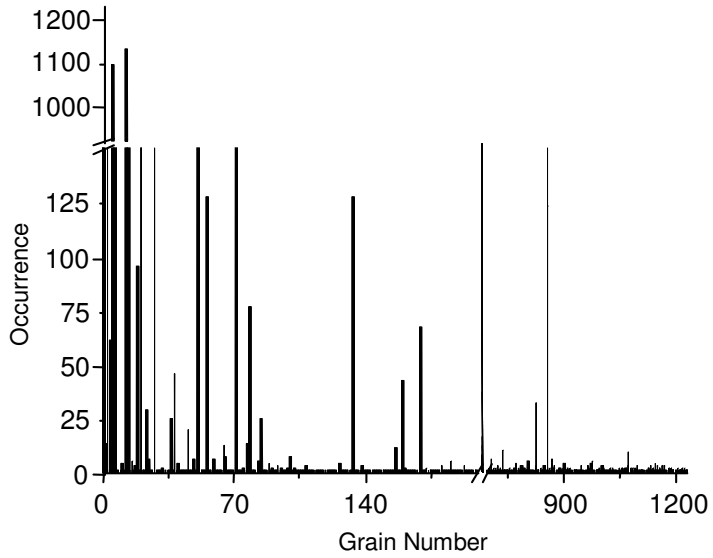

Figure 18 Histogram to determine the most frequently occurring grains.

Using this plot the top 16 grains with highest number of occurrences were chosen. In all, around 2000 different angular orientations with respect to the direction of the incident beam were observed. Most observed grains within the field of view, lie in the size range of 50-400μm across. From this initial sorting, evident information of the individual grain morphologies within the illuminated volume was observed. An illustration of the various grains as they appear in accordance with their orientation angles with respect to the incident beam is shown below.

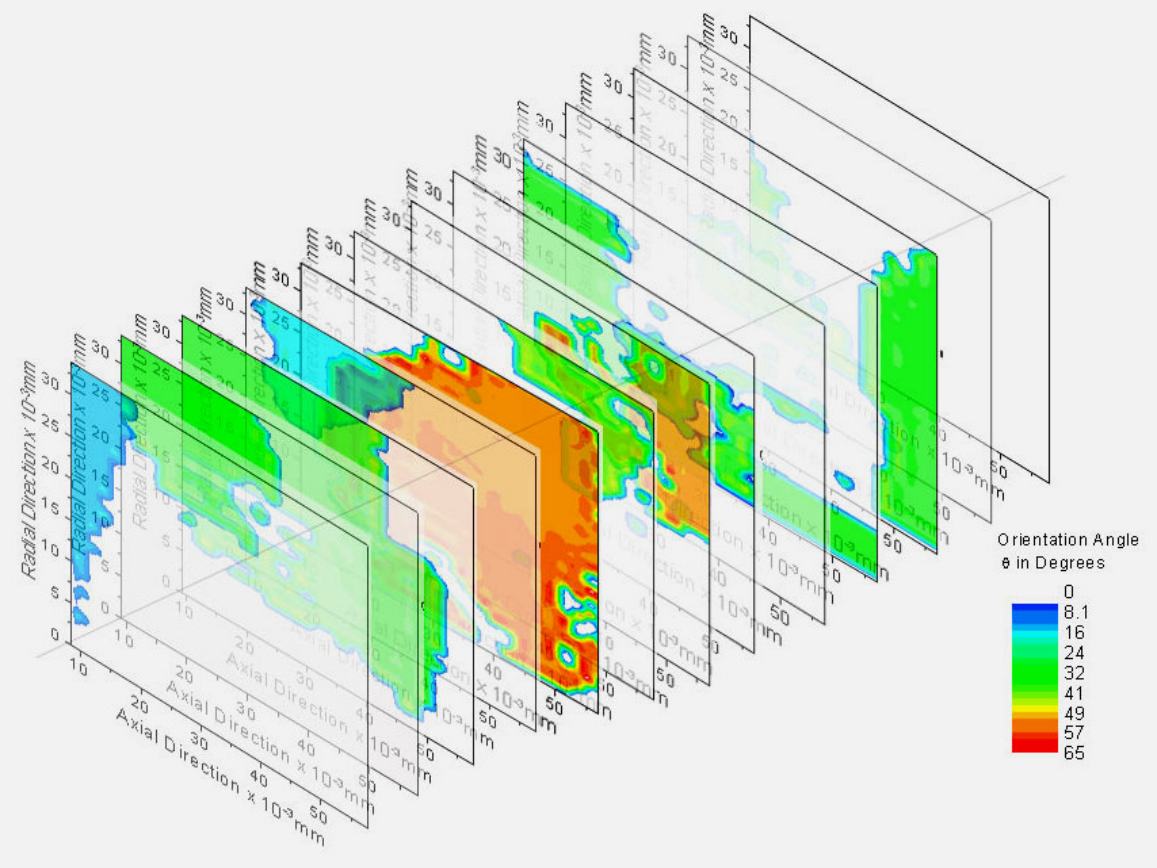

Figure 19 Grains with their respective orientation angles.

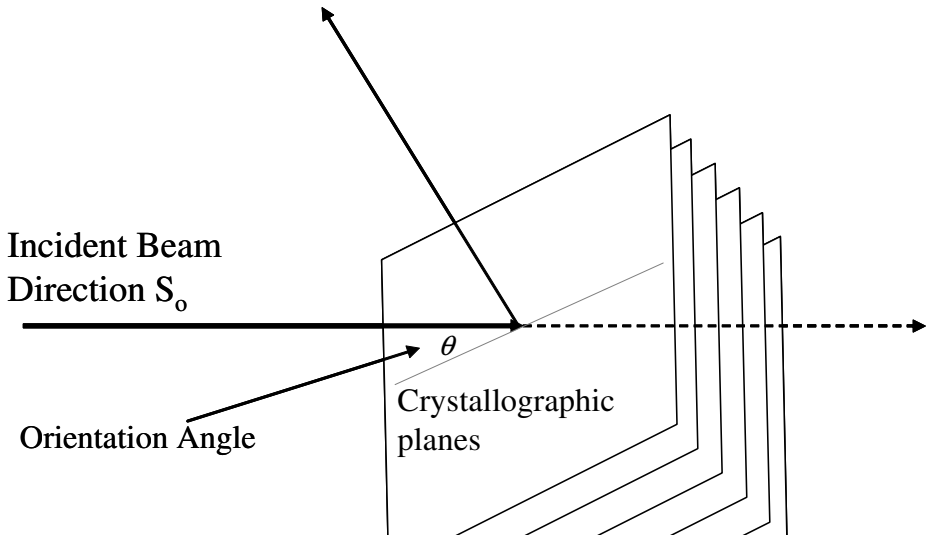

Figure 20 Schematic of the orientation angle of the grains

CHAPTER 6

6.0 RESULTS AND DISCUSSION

The first sets of measurements, primarily aim at measuring the residual strains, since no load is applied initially. Large differences in the coefficient of thermal expansion of the Aluminum matrix (2.34 $x10^{-5}$ $°C^{-1}$) and the Sapphire fiber ($4x10^{-6}$-- $8x10^{-6}°C^{-1}$) exists which result in the presence of significant residual strains in the matrix and the fiber. The effect of the large difference in coefficient of thermal expansion is brought about during the manufacture of the composite. Since the outer matrix is cast onto the preformed single crystal fiber, during the casting process the abovementioned residual strains are developed. The second aim is to study the effect of applied load on the existing residual strains. The measurements made at an applied load allow the understanding of the composite behavior in accordance to the load.

6.1 Microscopic Results

6.1.1 Strain Contours On Grains

The contour plots for the composite at 0 MPa and 80 MPa are shown below. The following are plots of the 16 most prominent grains chosen based on their occurrence, intensity and morphologies.

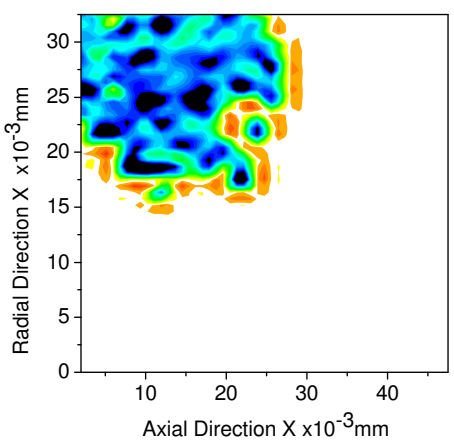

Strain at 0MPa # 1

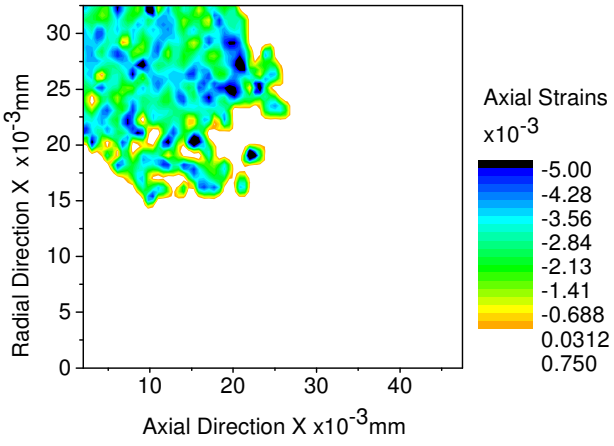

Strain at 80MPa #1

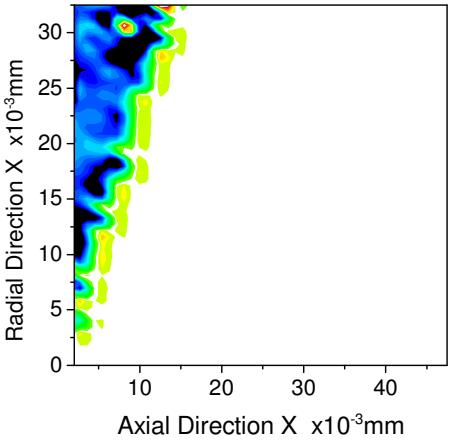

Strain at 0MPa # 2

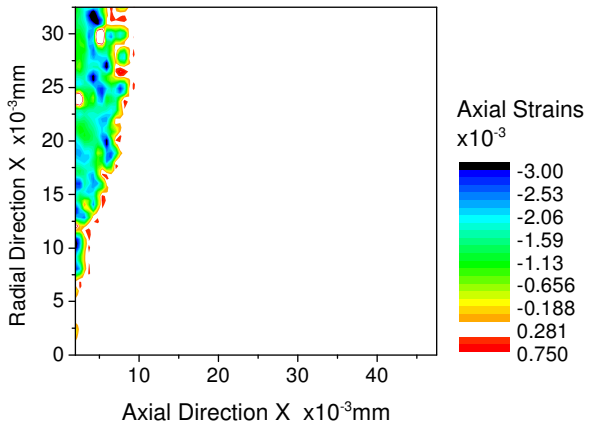

Strain at 80MPa # 2

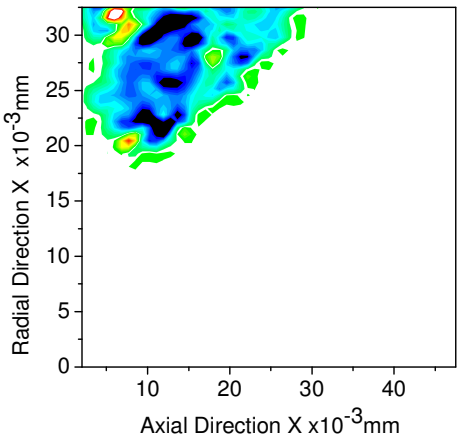

Strain at 0MPa # 3

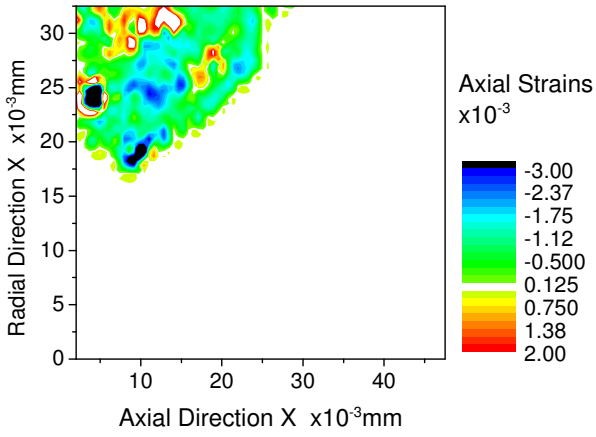

Strain at 80MPa # 3

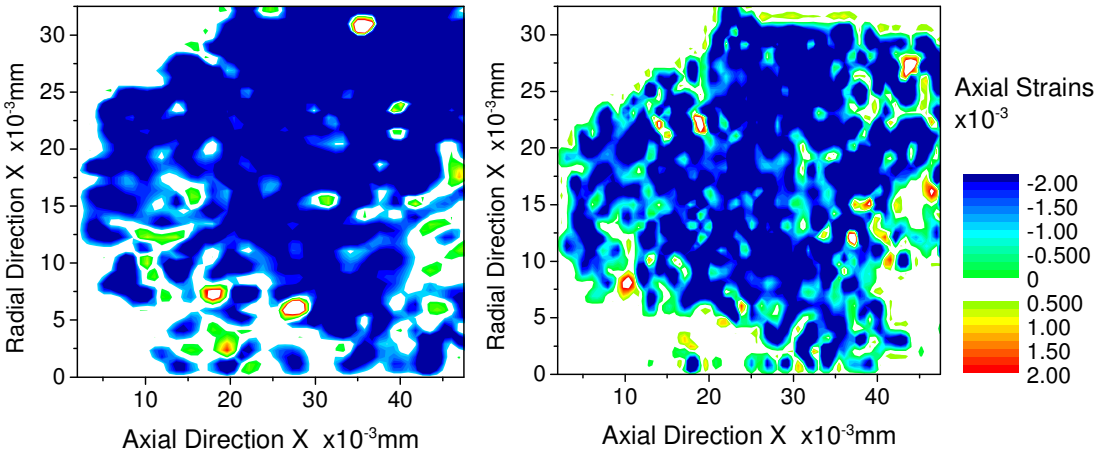

Strain at 0MPa # 4 Strain at 80MPa # 4

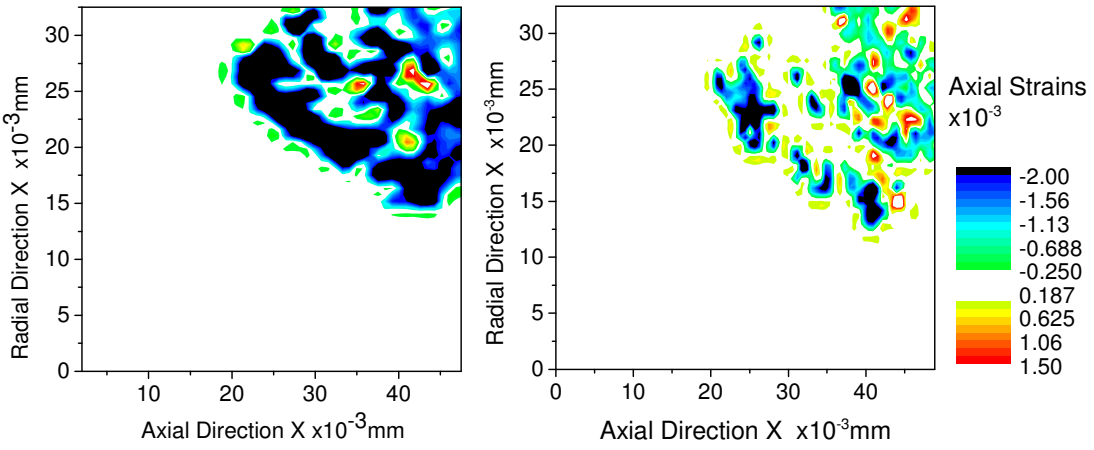

Strain at 0MPa # 5 **Strain at 80MPa # 5**

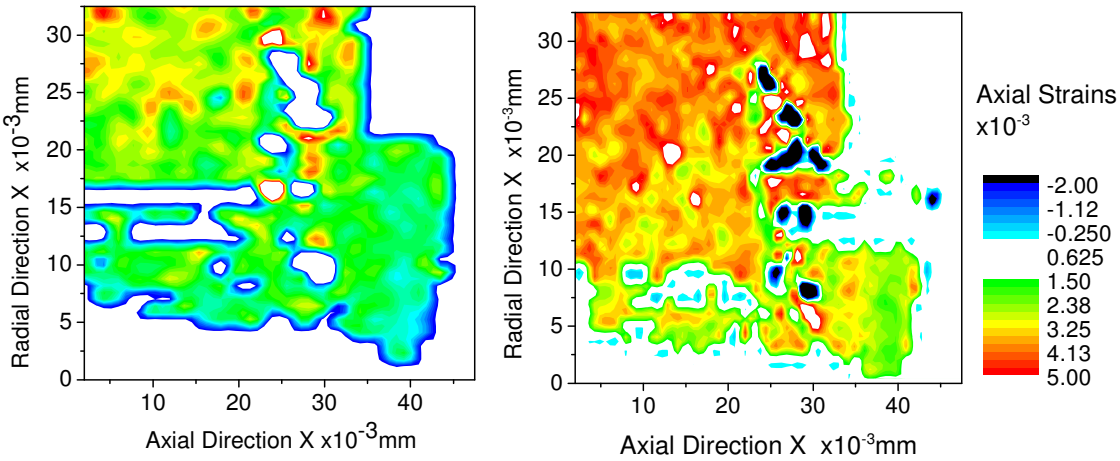

Strain at 0MPa # 6 **Strain at 80MPa # 6**

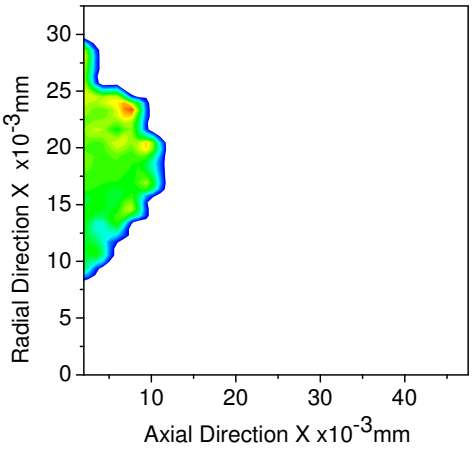

Strain at 0MPa # 7

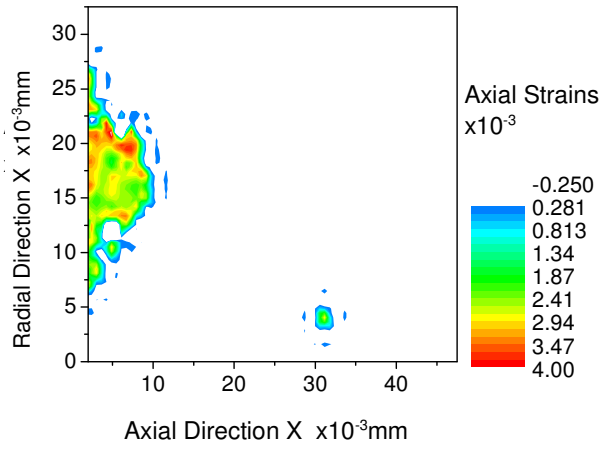

Strain at 80MPa # 7

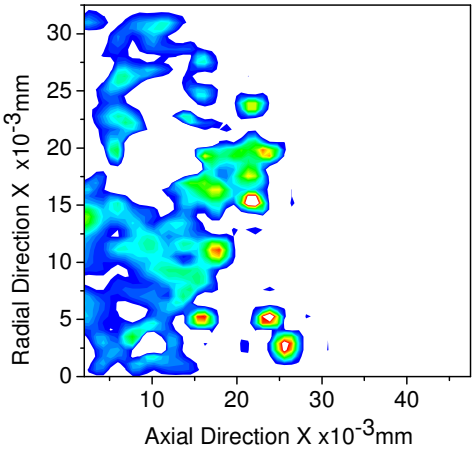

Strain at 0MPa # 8

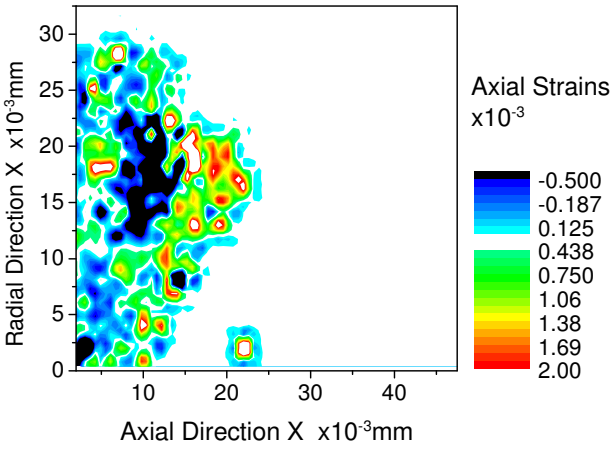

Strain at 80MPa # 8

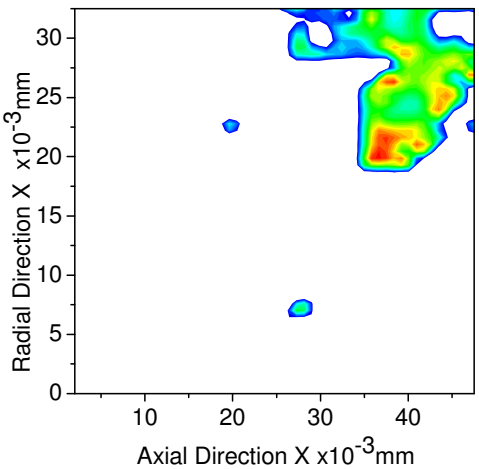

Strain at 0MPa # 9

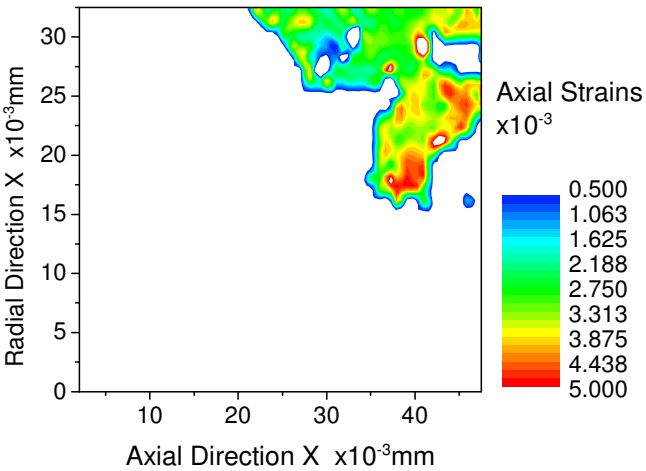

Strain at 80MPa # 9

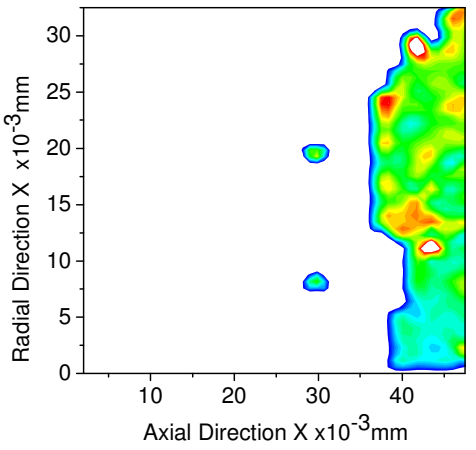

Strain at 0MPa # 10

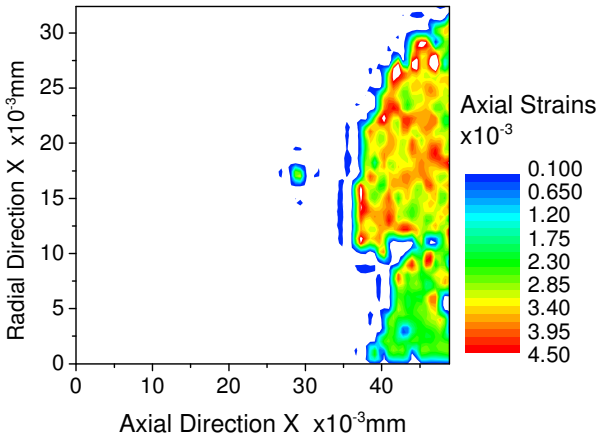

Strain at 80MPa # 10

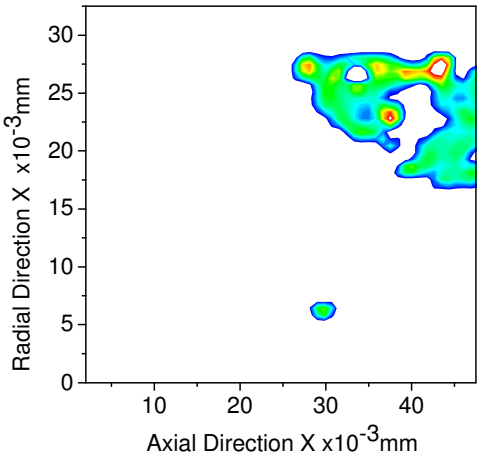

Strain at 0MPa # 11

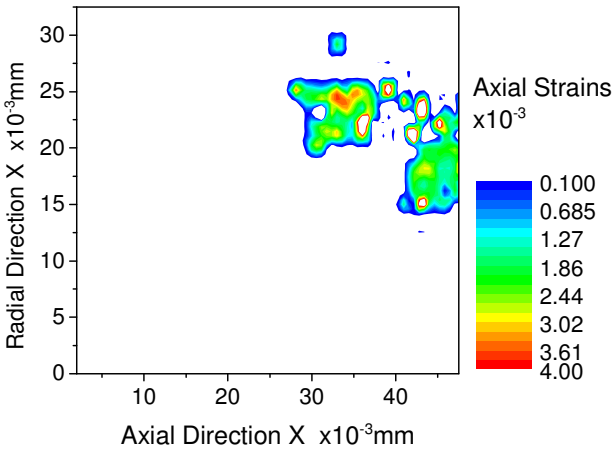

Strain at 80MPa # 11

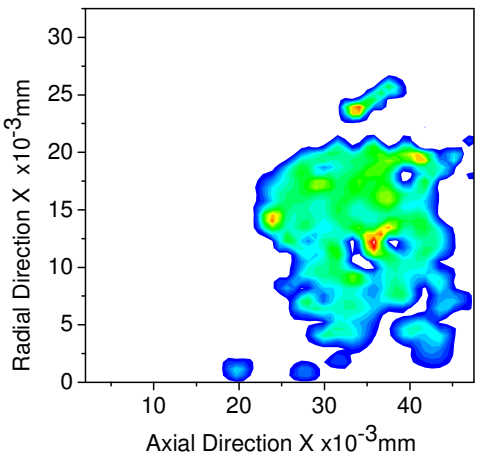

Strain at 0MPa # 12

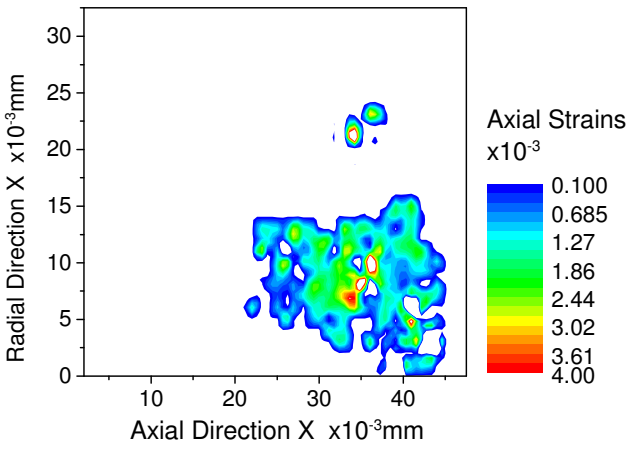

Strain at 80MPa # 12

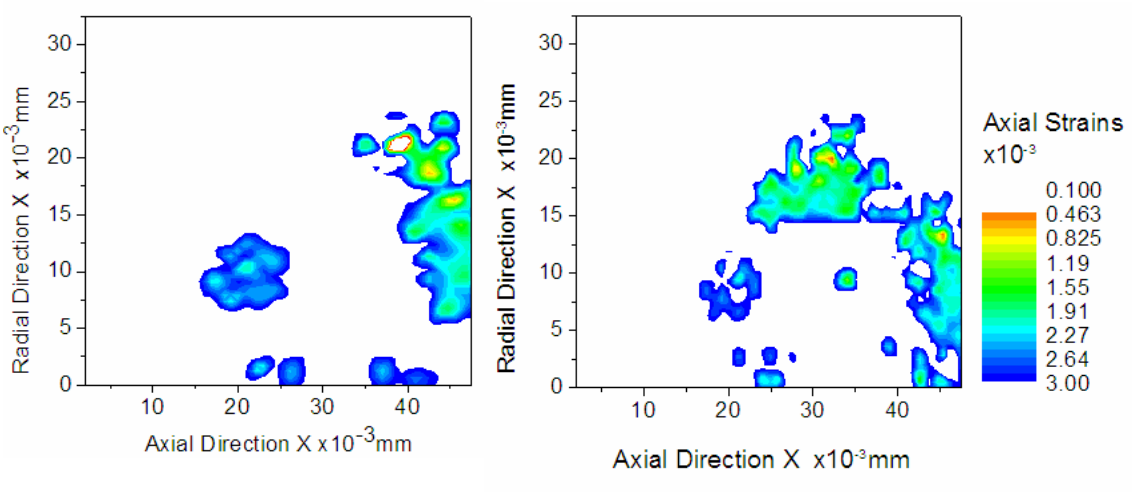

Strain at 0MPa # 13 **Strain at 80MPa # 13**

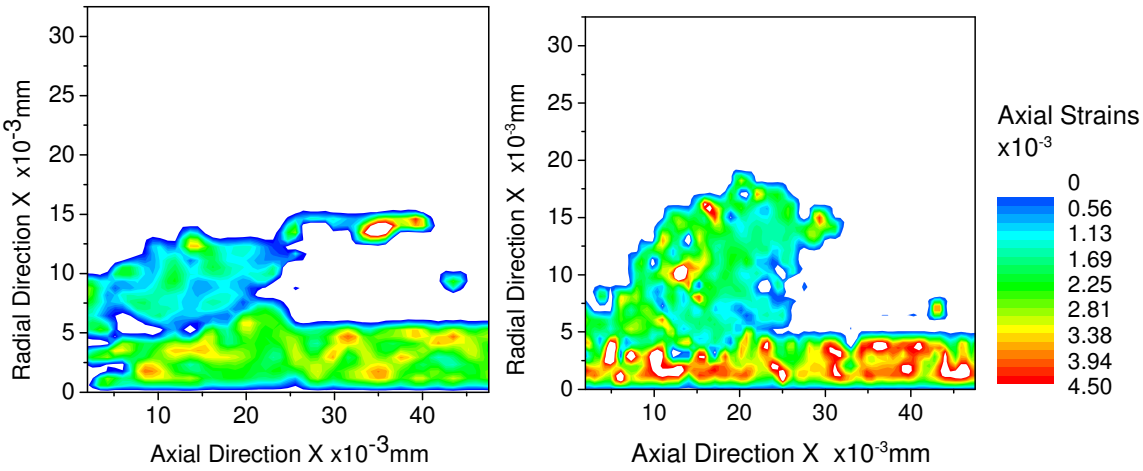

Strain at 0MPa # 14 **Strain at 80MPa # 14**

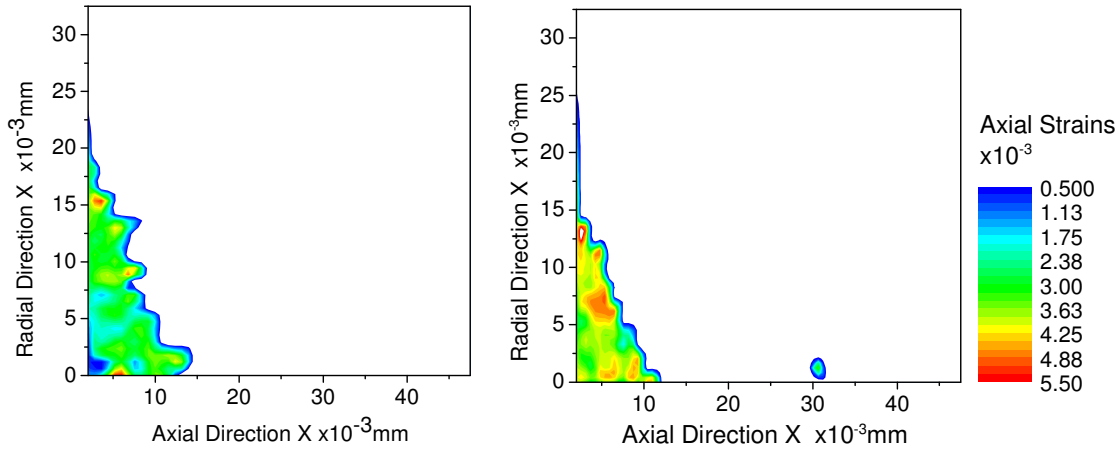

Strain at 0MPa # 15 **Strain at 80MPa # 15**

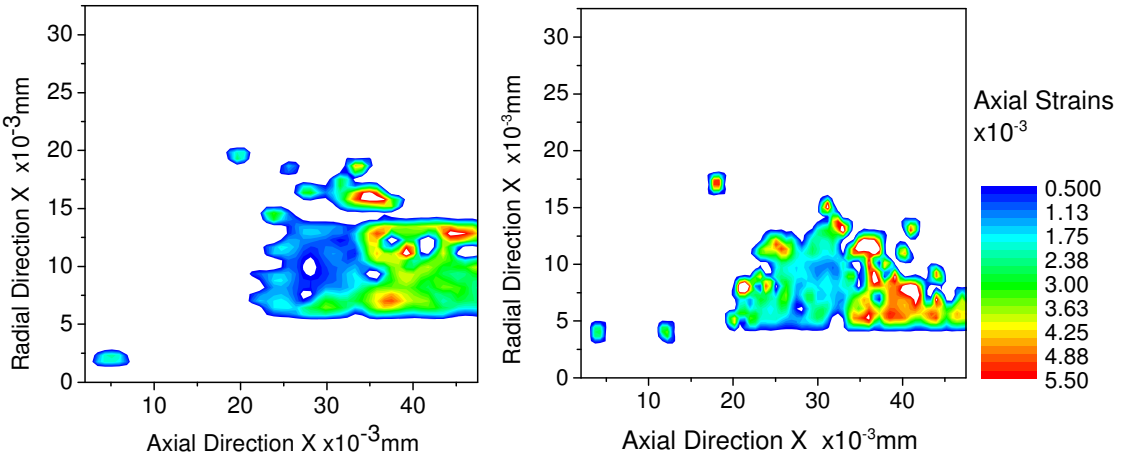

Strain at 0MPa # 16 **Strain at 80MPa # 16**

From figures for the grain # 1 - #16, the strain change is visible within the polycrystalline grains. A change in the morphology of the grain is seen with increase in load, but the overall geometrical shape is retained—which helps in recognizing the same grain across two different loads. A collection of the individual strain contours for individual grains has been arranged in a sequence to display the distribution of the grains in the field of view. This is illustrated in Figure 21.

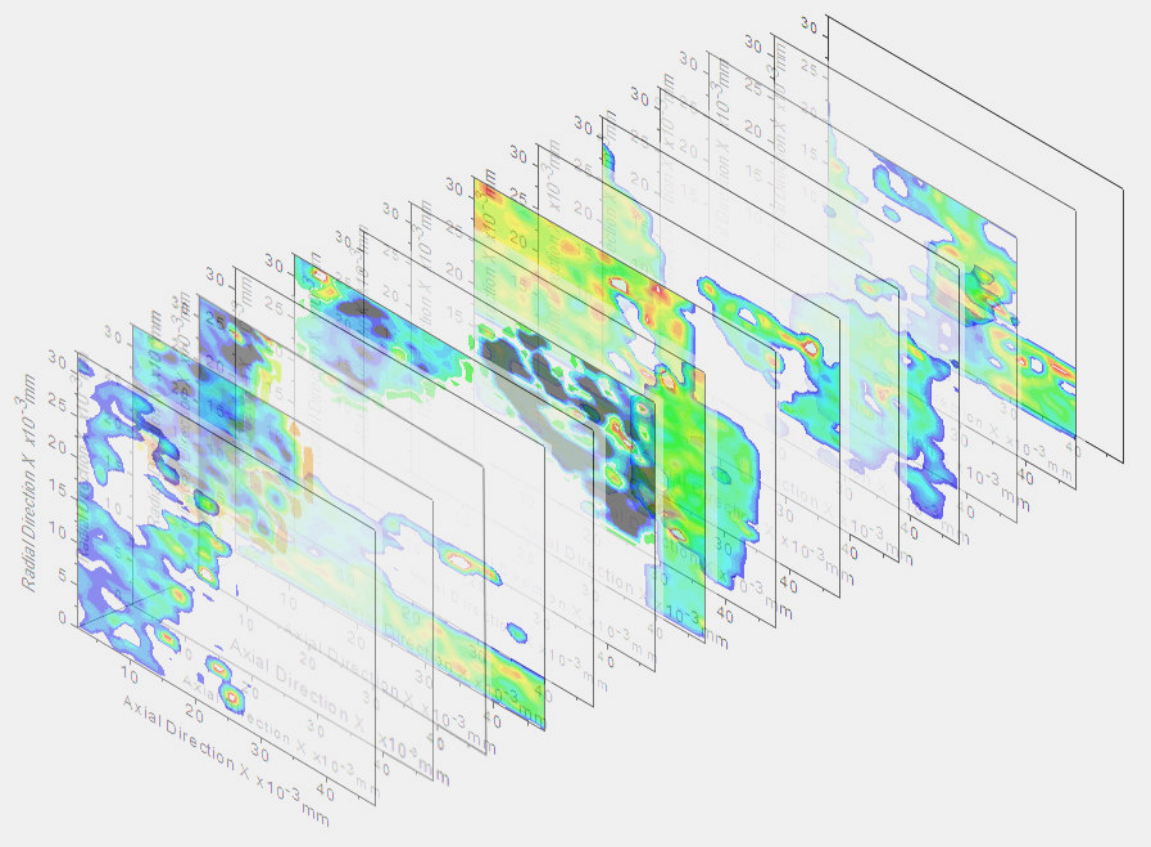

Figure 21 3-D stack of the scanned area. The individual contour plots cannot be arranged in order since the position of individual grain alongth the depth of the sample must only be evaluated using a triangulation technique. (Color Scheme for every frame is different and not shown in current image.)

6.1.2 Influence of the Fiber on the grains

Certain grains such as grain # 3, 13,14 & 16 can be seen to have a morphology which is flattened at the bottom where the fiber lies. The position of these grains in the x-y plane is near the vicinity of the axial fiber. The flattened shape of these grains can be attributed to their interaction with the fiber. The grains in the matrix are made up of cubic aluminum which is anisotropic in nature. Hence strains in all the different orientations of the matrix grains are different due to the corresponding stiffnesses in the respective directions.

An important fact that can be seen from the contour plots for grains (1, 2, 3, 5, 7 and 9) is that the grain initially exists in compression. Even loaded at 80 MPa the grains are found to be experiencing compression and hence some overall negative values over the contour region were observed. This stems from the anisotropic nature of the aluminum grains. Upon cooling from the melt some of the grains will be compressed by their neighbors whose contraction is less in that direction or whose stiffness is greater. The strain contours details each individual grain. Among the strain contours for the 16 grain, plots for grain # 6, 8, 9, 11, 12, 13, 16 can be seen to have discrete isolated areas which are separated from the main grains. These little islands are parts of other grains which show up along with the main grains because of similar crystal orientation. These islands do not necessarily indicate the whole grain, but may be a part of the deeply located diffracting sub-grain.

6.1.3 Strain Plots along the fiber.

Strain contour plots similar to the ones implemented for the polycrystalline matrix are plotted for the single crystal sapphire fiber. The strain variation in the fiber across the two loads is compared in the following figures. The following plots show a grey area which is occupied solely by the matrix and the colored region indicates the magnitude of axial strains present in the fiber (within the matrix) at no applied load and at a load of 80MPa.

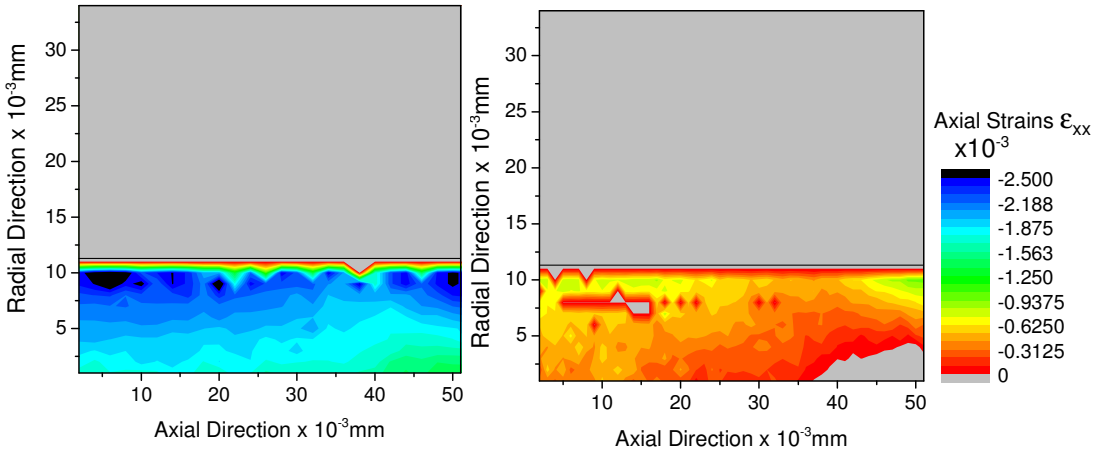

Strain at 0MPa # 17 **Strain at 80MPa # 17**

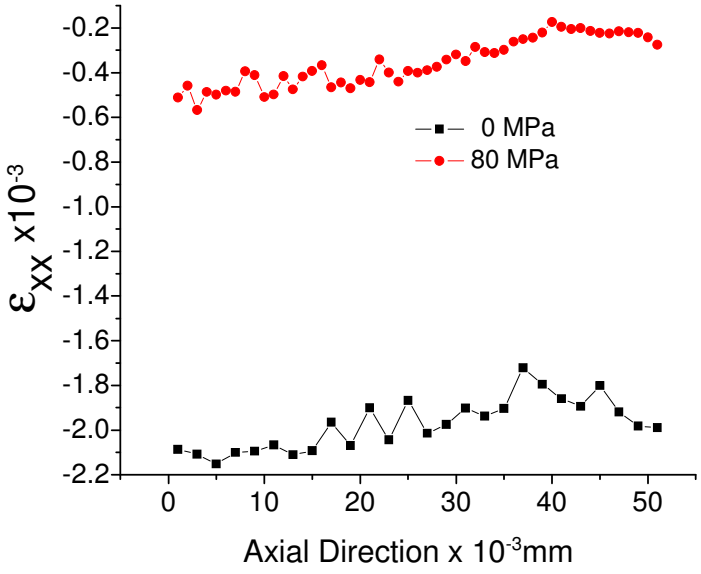

Figure 22 Radially averaged Axial Strain ε_{xx} change across applied load.

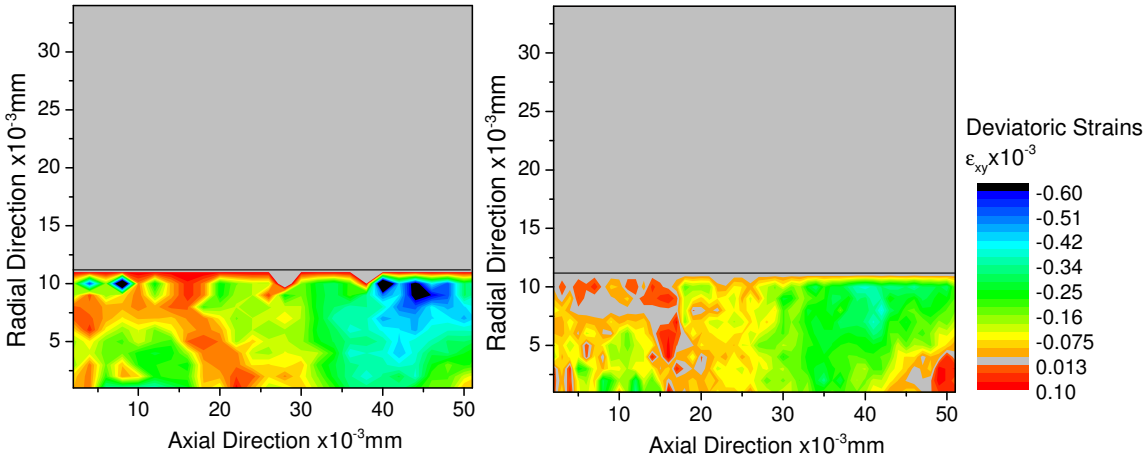

Strain at 0MPa # 18 **Strain at 80MPa # 18**

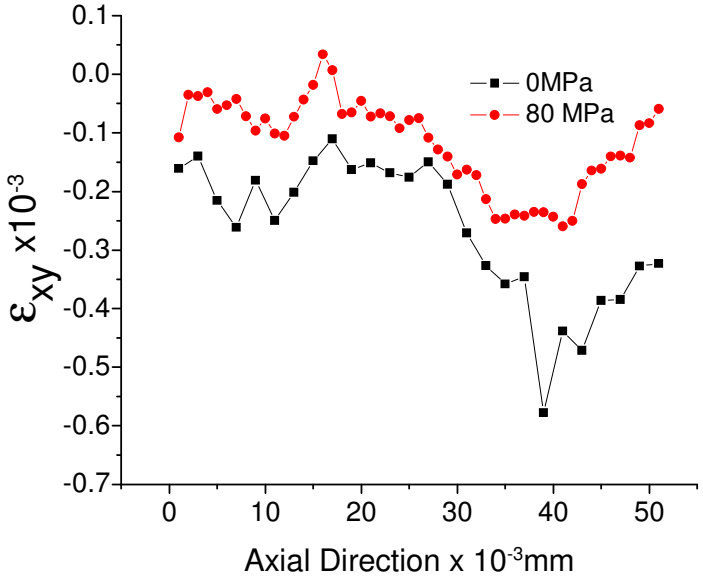

Figure 23 Radially averaged Deviatoric Strain ε_{xy} change across applied load.

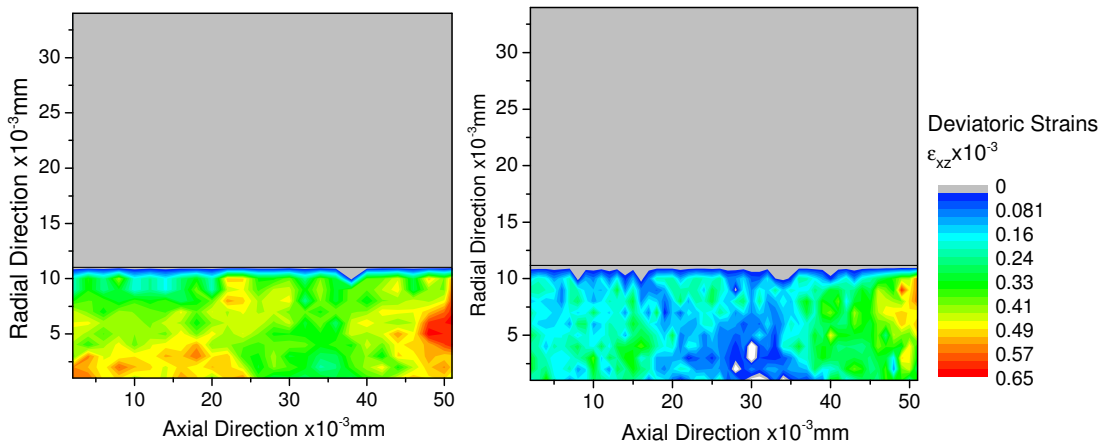

Strain at 0MPa # 19 **Strain at 80MPa # 19**

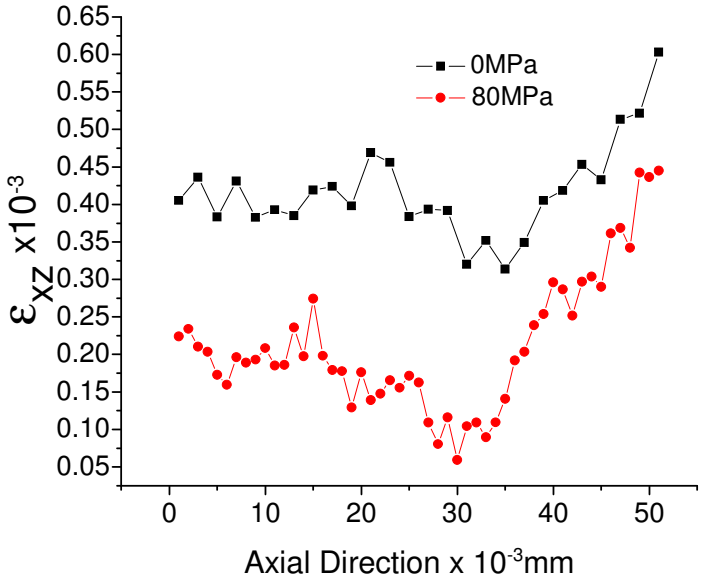

Figure 24 Radially averaged Radial Strain ε_{xz} change across applied load.

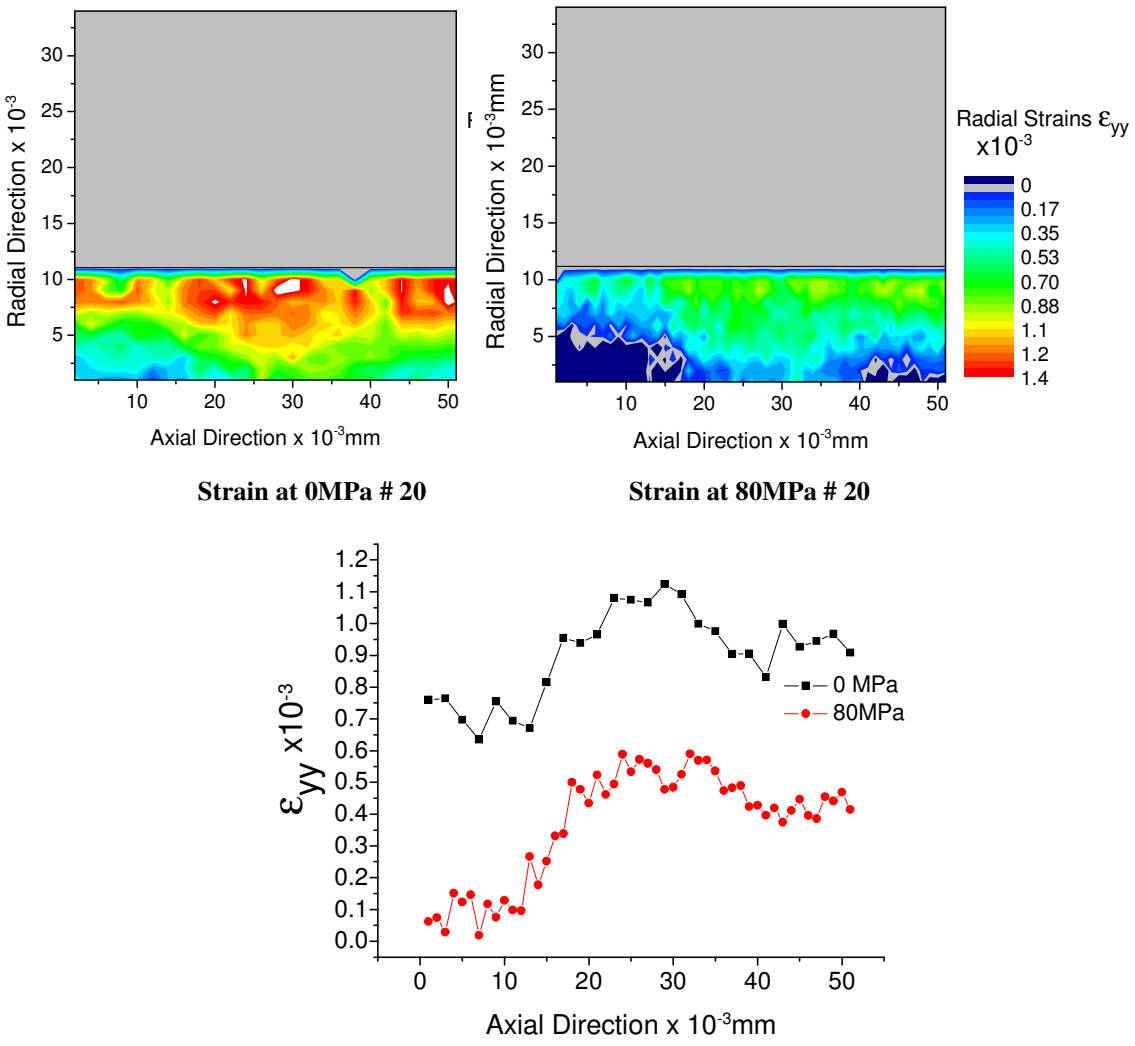

Figure 25 Radial Strain ε_{yy} change across applied load.

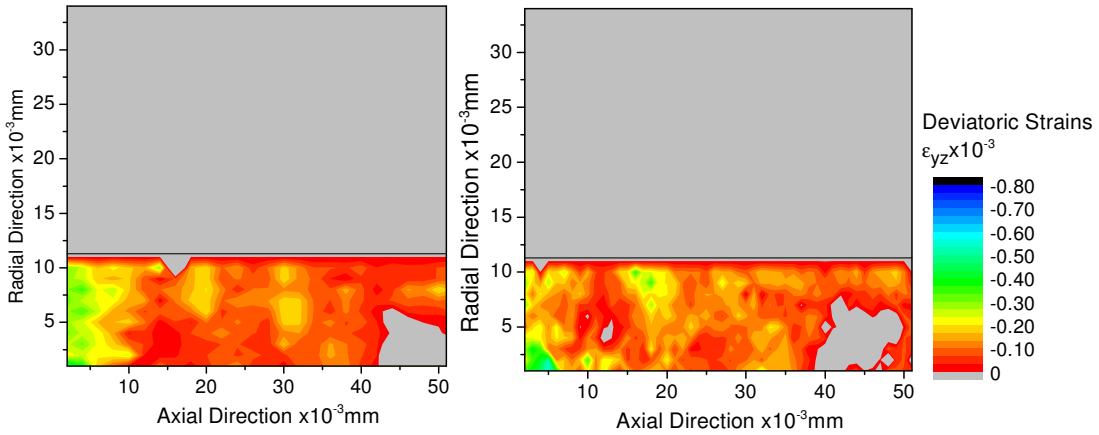

Strain at 0MPa # 21 **Strain at 80MPa # 21**

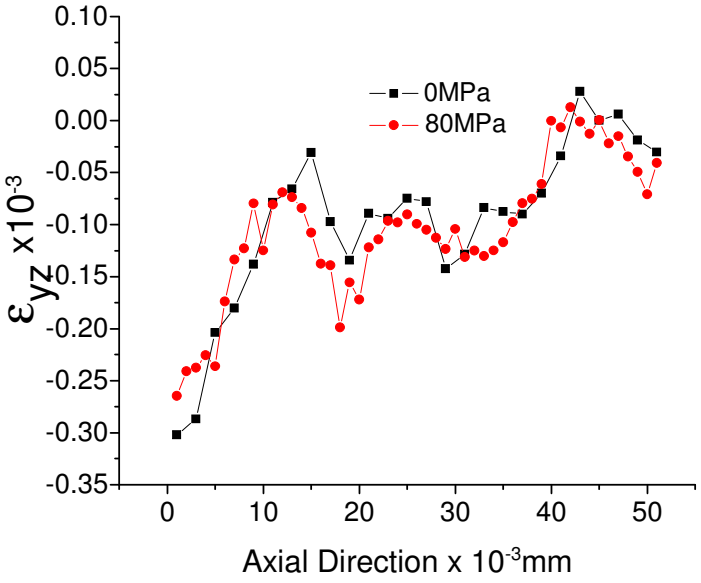

Figure 26 Deviatoric Strain ε_{yz} change across applied load.

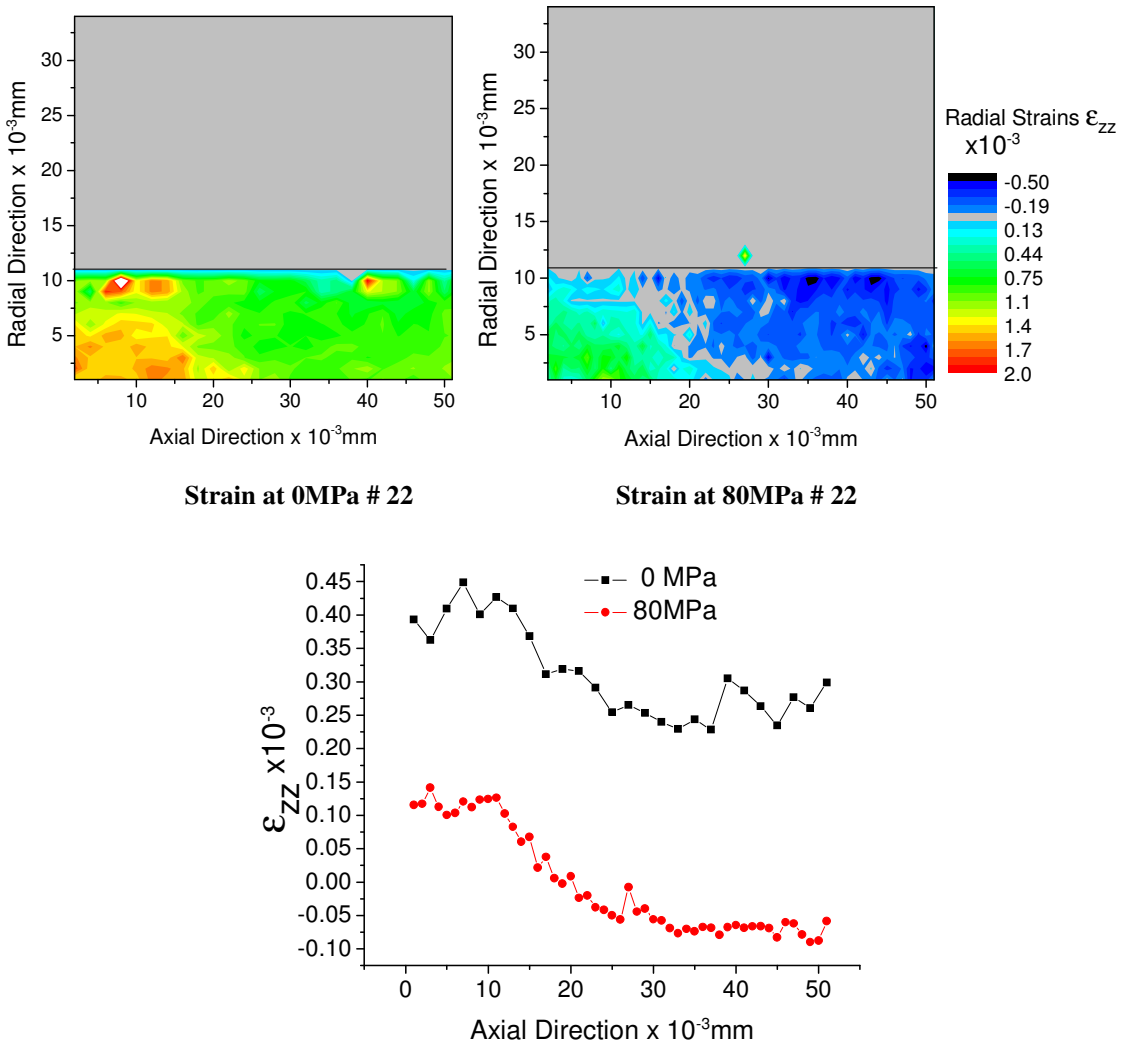

Figure 27 Radial Strain ε_{zz} change across applied load.

While the fiber is also anisotropic, since there is only one fiber crystal, the observed non-uniform residual strains are caused by the matrix surrounding the fiber. Variations in the residual strain along the fiber are due both to the anisotropic nature of the surrounding aluminum grains, inconsistencies in the matrix (such as voids), and possible variations in the fiber-matrix interface.

6.2 Macroscopic Result

Integrated Effect of the Grains

The various grains seen above have been assigned an index number for conveniently recognizing the grains. Further, the strains across each grain observed are averaged over the grain's total area. This assists in objectively distinguishing the strains and conducting a statistical comparison. The grouped data relating the two load conditions for every individual grain is given in Table 1.

Table 1 Strain Change due to applied stress for the grains under consideration

	Load = 0 MPa	Load = 80 MPa	
Grain #	Axial Strain Єxx	Axial Strain Єxx	Change in Strain
0	-0.4384	0.23192	0.20645
1	-2.542	-1.6832	0.85876
2	-4.0841	-3.1695	0.91467
3	2.33376	3.11496	0.7812
4	-1.7406	-0.8184	0.92215
5	-2.5536	-2.2721	0.2815
6	2.70559	3.17327	0.46768
7	-1.8719	-0.9311	0.94081
8	2.4438	3.22965	0.78585
9	-0.3471	0.3337	0.01337
10	2.61864	3.17488	0.55624
11	2.20782	2.52954	0.32172
12	1.64118	1.61141	0.02977
13	0.94604	1.5727	0.62666
14	1.85436	2.54958	0.69522
15	2.92048	3.7923	0.87182
16	2.51357	3.40827	0.8947

The grains were grouped at the two different load conditions and a graphic representation of the above is shown in Figure 28. The nature of the distribution of the grains suggests that grains with unique values of strains are scattered in a specific order along the strain direction. A co-relation with the Reuss Model [71] for calculation of bulk elastic constants could be made. It is observed from the Figure 28, that a substantial number of grains are stacked towards the positive strain side. This distribution of the strains suggests that the experimental results do not co-relate to the assumptions of neither the Voigt model nor the Reuss model which are based on uniform strain and stress respectively [6].

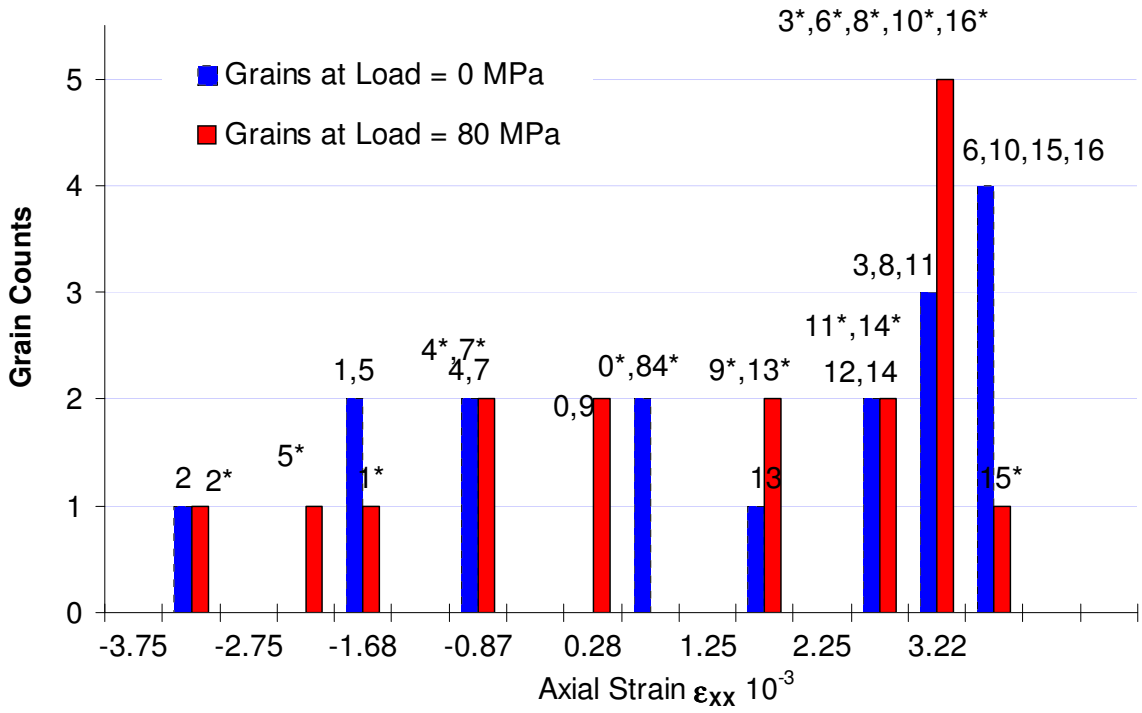

Figure 28 Histogram of the strains observed in each grain at applied stress of 0MPa and 80MPa

The stacking of more grains towards the positive strain side after applied stress indicates a particular nature in which the grains behave under tensile loading condition.

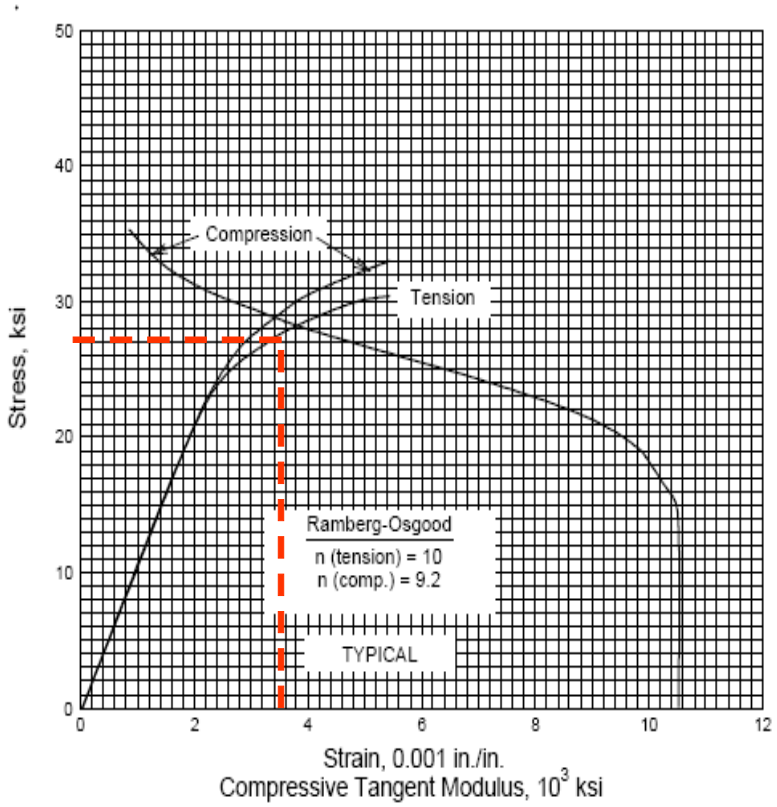

Figure 29 Stress Strain Curve for Aluminum depicting the elastic region.

Figure 29 shows the tensile stress-strain curve of Aluminum A356. The dashed red lines on the plot enclose the strains and the corresponding stresses as observed from the experimental results. Most strains as seen in Figure 29 lie in the region where the red line is marked. The red line shows the highest strain which exists in the matrix which is almost equal to 3.8×10^{-3}. The corresponding intercept on the curve suggests that some grains are under plastic deformation. This fact can be realized through the observation of diffraction spots obtained at the second applied load of 80MPa. The spots appear broadened or (smeared) as compared to their initial state. This smearing of the

diffraction spots is attributed to the yielding taking place in some grains. The smearing stems from a distribution of lattice spacing in the metal caused by mechanisms such as dislocation pileup during plastic deformation. A smeared spot is shown in Figure 30.

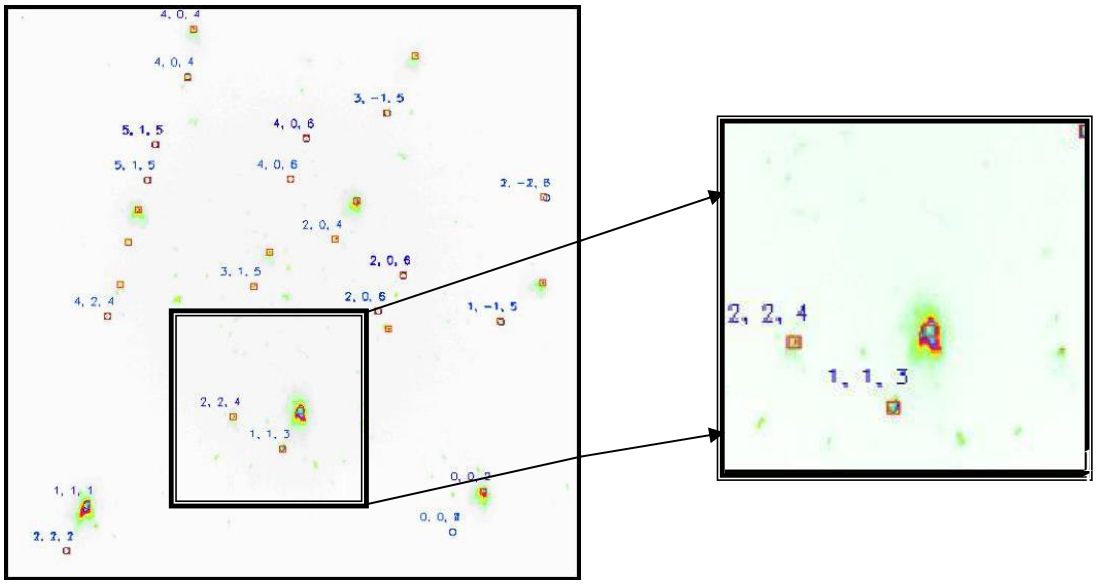

Figure 30 Image of Diffraction Spots obtained at 80 MPa showing yielding indicated by the smeared spots.

6.3 Residual Strain Distribution

A plot of the residual strain distribution along the fiber integrating the effect due to all the grains in the field of observation of the matrix region of the sample is shown in Figure 31. The figure consists of all the data points which have corresponding residual strain values in the matrix along the fiber length (no grain classification has been made). The distribution of strains in all the grains (about 2000) can be observed in the figure. Figure 32 is a similar plot indicating the distribution of deviatoric strains in the plane parallel to the axial direction.

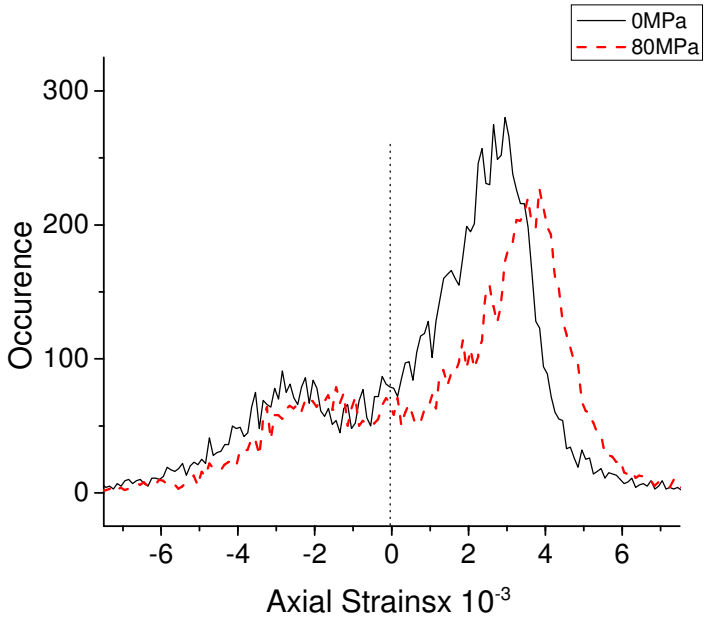

Figure 31 Bimodal distribution of the axial strains in the matrix grains.

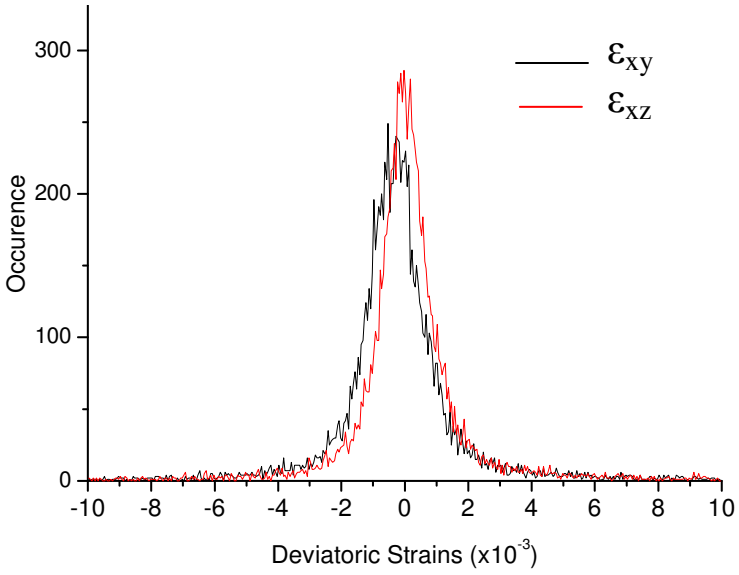

Figure 32 Distribution of the shear strains in the matrix at 0 MPa

The distribution of the deviatoric strains is seen to be evenly distributed about zero strain which indicates that the preference for residual shear strains is not distinctly seen as compared to the bimodal distribution of the axial strains as seen in Figure 31.

The X-ray measurement scans on the sapphire fiber and the aluminum matrix were separated and the resulting effect of the load on the fiber and the matrix can be seen at the two load steps. Figure 33 shows the residual stresses that existed along the axis of the fiber prior to loading. Using the "energy scan" method along the fiber axis, the actual calibrated strains referenced to a strain free reference in the fiber were observed. An average residual strain of -2.53 x 10^{-3} was observed.

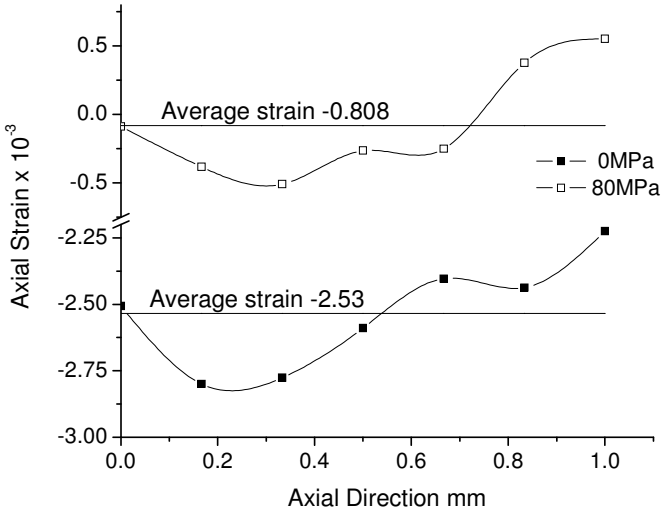

Figure 33 Axial residual strains present in the center of the fiber and strains resulting from applied stress.

The measured average axial strain in the fiber after loading the composite sample to an applied stress of 80Mpa was -0.81x10^{-3}.

The plot in Figure 34 shows the change in the overall average axial strains along the length of the fiber for grain "15." The applied stress has shifted the strains in tension. This grain has the highest average strain among the 20 largest grains considered. It can be inferred from this plot that the grain is present in the 0-0.3mm section. The strain

average along the axial direction is calculated at the two loads. The grain with the strain comparison is seen in the background.

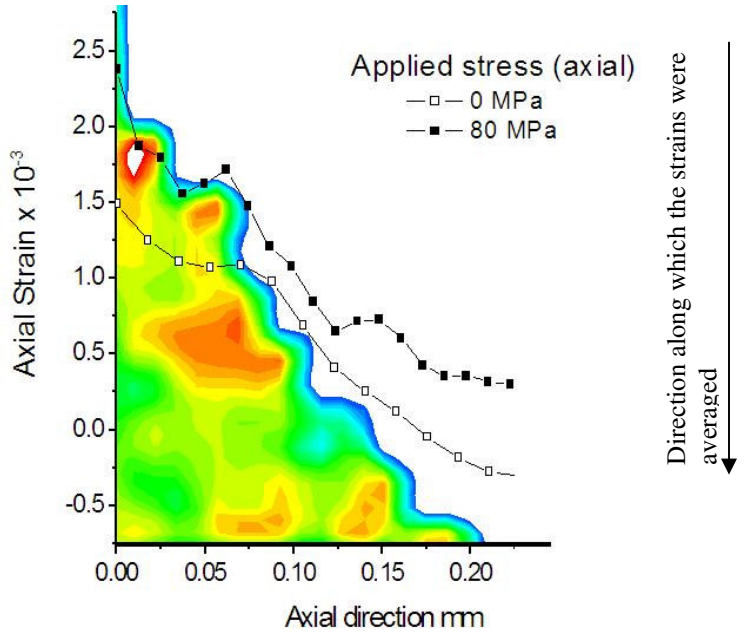

Figure 34 Axial strains averaged radially in Grain#15 at 0 Mpa and at 80 MPa (lines) over the contour plot at 80 MPa applied stress in the background

CHAPTER 7

7.0 CONCLUSIONS

The micro-Laue X-ray diffraction method has been used to look into the behavior of the aluminum matrix embedded with a sapphire single crystal fiber at a sub-micron level. An overall perspective of the interactions of the grains within the matrix and the reinforcing fiber was obtained. The use of polychromatic light, unlike conventional monochromatic techniques, presented data from a significantly greater number of grains than available with monochromatic light. A major advantage of using this technique for strain measurement is the individual identification of grains at each applied stress.

The morphology, orientation, and relative strain data was sufficient to identify individual grains after application stress. The inter-granular strains were observed for 16 grains and the single crystal fiber before and after applied stress. Also obtained, are the inter-fiber strains which are present due to the interaction of the fiber and the grains at the interface.

A method of averaging micro-beam strain results to obtain average grain-specific strains was also determined and applied to observe the distribution of strains within the matrix. A new method, analogous to the Bragg-edge technique, of calibrating absolute *d*-spacing and thus residual strains was described. Its application provided for observation at a sub-micron scale of the full strain tensor across a wide field of view. The axial residual strain

in the fiber due thermal expansion mismatch was observed as an average of -2.5 x 10^{-3} with considerable variation along the axis of the composite due to the fiber matrix interface, the anisotropic nature of the surrounding aluminum grains, and inconsistencies in the matrix (such as voids).

The micro-Laue technique has provided a visual insight by providing two-dimensional representation of the grains contoured by strain. The current results, express the grains in a plane. The position of every grain in a volume by triangulation would allow understanding of the interaction of the matrix with the fiber. The distribution of the residual stresses in the matrix and fiber has been categorized, allowing a better visualization of the internal stress state in a model metal matrix composite.

CHAPTER 8

8.0 FUTURE DEVELOPMENTS

The analysis carried out in the current experiment considers the grains in the scope of the beam. The positions of these grains are, so far, specified in the X and Y absolute coordinates which are with reference to the sample. The exact location of the depth of the grain within the illuminated volume of the sample is not yet determined. This could be done using triangulation techniques wherein the diffraction patterns are recorded on the CCD which is moved away from the sample in the direction of the diffracted beam. Data of each diffraction spot corresponding to the position of the CCD is noted. Once a suitable number of data points have been recorded, the diffracted beam path can be extrapolated to determine the depth of the grain which is diffracting the beam. New techniques such as the 3D X-ray diffraction Microscope using a moving wire [72] can provide alternatives in verifying results obtained using the triangulation diffraction technique. Furthermore, as discussed in the literature review, the technique used to determine grain boundaries could also be combined with the above techniques to measure the entire idea of grain-to-grain interaction in 3D.

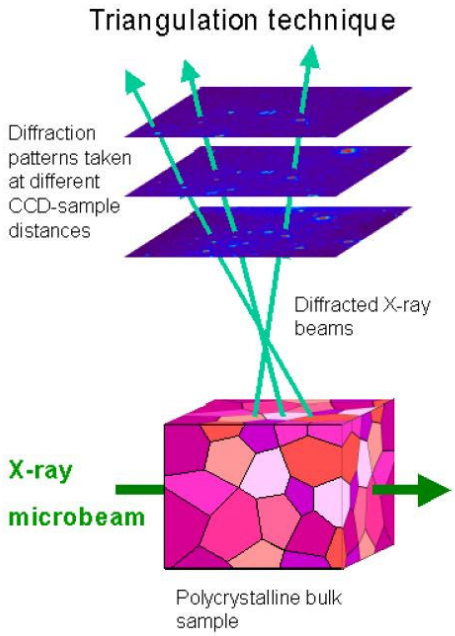

Figure 35 Schematic of the Triangulation Technique for Grain Location in 3D.

The current work has been restricted to the elastic effects on the grain. An analysis of the data available for further loading of the sample could provide better understanding of plastic deformations and the strain states, and information on predicting composite failure. Analysis of diffraction spot shapes and self-consistent models will allow plastic deformation studies. The 3-Dimentional position of the grains will also be invaluable in determining fiber matrix interface characteristics.

References

1. Daniel, I. M., Ishai, O., *Engineering Mechanics of Composite Materials*. Oxford University Press, Inc. New York, NY,1994; 4.

2. Suresh, S., Mortensen, A., Needleman, A., *Fundamentals of Metal-Matrix Composites*. Butterworth-Heinemann, Stoneham, MA, 1993; 307, 313.

3. Hanan J. C., "Damage Evolution in Uniaxial SiC Fiber Reinforced Ti Matrix Composites," *Ph.D. Thesis, Materials Science and Engineering Option, California Institute of Technology*, 2002.

4. He, J., Beyerlein, I. J., Clarke, D. R., "Load Transfer From Broken Fibers in Continuous Fiber Al2O3-A1 Composites and Dependence on Local Volume Fraction." *J. Mech. Phys. Solids*, 1999; 47 (3): 465-502.

5. MacDowell, A.A., Celestre, R.S., Tamura, N., Spolenak, R., Valek, B., Brown, W. L., Bravman, J. C., Padmore, H. A., Batterman, B. W., Patel, J. R., "Submicron X-ray diffraction", *Nuclear Instruments and Methods in Physics Research* A 467–468 2001, 936–943.

6. Noyan, I. C., Cohen, J. B., *Residual Stress*. Springer-Verlag, New York, 1987.

7. *ASTM Standards and Literature References for Composite Materials*, 2nd Ed., American Society for Testing and Materials, Philadelphia, PA, 1990.

8. Maire E., Owen A., Buffiere J. Y. And Withers P. J., "A Synchrotron X-Ray Study Of A Ti/SiC Composite During In Situ Straining", *Acta mater.* 49 2001, 153–163.

9. John G. Goedjen, David A. Shores, James H. Stout, "In-situ strain measurements in the Ni/NiO system during high temperature oxidation", *Materials Science and Engineering,* A 222 1997, 58-69.

10. Epstein J.S., Deason V. A., Reuter W. G., "On the Determination of Elastic Residual Strain Fields in Rail Wheels Using Moire Interferometry", *Optics and Lasers in Engineering 12* 1990 189-201

11. Ginesu F., "Application of the holographic Moiré technique to the analysis of composite materials", *Measurement,* Vo1.10 No 2, Apr-Jun 1992.

12. Tay T. E., Yap C. M., Tay C. J., "Crack Tip And Notch Tip Plastic Zone Size Measurement By The Laser Speckle Technique", *Engineering Fracture Mechanics* Vol. 52, No. 5, Pp. 879-893, 1995.

13. Hubert A. Aebischer & Stephan Waldner, "Strain Distributions made Visible with Image-shearing Speckle Pattern Interferometry", Optics and Lasers in Engineering 26 1997, 407-420.

14. Steinchen W., Kupfer G., Mäckel P., Vössing F., "Determination of strain distribution by means of digital shearography", *Measurement*, 26 1999, 79–90.

15. Kohji Toda, Goro Sugizaki, Tadashi Takenaka and Koichiro Sakata, "A technique for measuring strain in layered structure media", *Sensors and Actuators, A,* 43 (1994) 213-216.

16. Hanan, J. C., Ustundag, E., Clausen, B., Sivasambu, M., Beyerlein, I. J., Brown, D. W., Bourke, M. A. M. "Residual Strain Evolution During the Deformation of Single Fiber Metal Matrix Composites." *Materials Science Forum*. 2002; 404-4: 907-911.

17. Wagner, H. D., Amer, M. S., Schadler, L. S., "Fibre Interactions in Two-Dimensional Composites by Micro-Raman Spectroscopy." *J. Mat. Sci.*, 1996; 31 (5): 1165-1173.

18. Van den Heuvel, P. W. J., Peijs, T., Young, R. J., "Failure phenomena in two-dimensional multi-fibre microcomposites .2. A Raman Spectroscopic Study of the Influence of Inter-Fiber Spacing on Stress Concentrations." *Compos. Sci. Tech.*, 1997; 57 (8): 899-911.

19. Beyerlein, I. J., Amer, M. S., Schadler, L. S., Phoenix, S. L., "New Methodology for Determining In Situ Fiber, Matrix and Interface Stresses in Damaged Multifiber Composites." *Sci. Eng. Compos. Mat.*, 1998; 7 (1-2): 151-204.

20. Schadler, L. S., Amer, M. S., Iskandarani, B., "Experimental Measurement of Fiber/Fiber Interaction Using Micro Raman Spectroscopy." *Mechanics of Materials*, 1996; 23 (3): 205-216.

21. Cullity, B. D., *Elements of X-Ray Diffraction*. 2nd ed. Addison Wesley, Massachusetts, PA, 1978; 130, 464-475.

22. Vogel S., Ustundag E., Hanan J. C., Yuan V.W. , Bourke M.A.M., "In-situ investigation of the reduction of NiO by a neutron transmission method", *Materials Science and Engineering* A333 (2002) 1–9.

23. Dragoi, D., Ustundag, E., Clausen, B., Bourke, M. A. M. "Investigation of Thermal Residual Stresses in Tungsten- Fiber/Bulk Metallic Glass Matrix Composites." *Scr. Mater.* 2001; 45(2): 245-252.

24. Choo, H., Rangaswamy, P., Bourke, M. A. M., Larsen, J. M. "Thermal Expansion Anisotropy in a Ti-6al-4v/Sic Composite." *Mater. Sci. Eng. A-Struct. Mater. Prop. Microstruct. Process.* 2002; 325(1-2): 236-241.

25. Carter, D. H., Bourke, M. A. M. "Neutron Diffraction Study of the Deformation Behavior of Beryllium-Aluminum Composites." *Acta Mater.* 2000; 48(11): 2885-2900.

26. Rangaswamy, P., Daymond, M. R., Bourke, M. A. M., Von Dreele, R., Bennett, K., Jayaraman, N. "Texture and Residual Strain in Two Sic/Ti-6-2-4-2 Titanium Composites." *Metall. Mater. Trans. A-Phys. Metall. Mater. Sci.* 2000; 31(3A): 889-898.

27. Choo, H., Rangaswamy, P., Bourke, M. A. M. "Internal Strain Evolution During Heating of Ti-6al-4v/Scs-6 Composite." *Scr. Mater.* 1999; 42(2): 175-181.

28. Warrier, S. G., Rangaswamy, P., Bourke, M. A. M., Krishnamurthy, S. "Assessment of the Fiber/Matrix Interface Bond Strength in Sic/Ti-6al-4v Composites." *Mater. Sci. Eng. A-Struct. Mater. Prop. Microstruct. Process.* 1999; 259(2): 220-227.

29. Rangaswamy, P., Bourke, M. A. M., Wright, P. K., Jayaraman, N., Kartzmark, E., Roberts, J. A. "The Influence of Thermal-Mechanical Processing on Residual Stresses in Titanium Matrix Composites." *Mater. Sci. Eng. A-Struct. Mater. Prop. Microstruct. Process.* 1997; 224(1-2): 200-209.

30. Allen, A. J., Bourke, M. A. M., Dawes, S., Hutchings, M. T., Withers, P. J. "The Analysis of Internal Strains Measured by Neutron- Diffraction in Al-Sic Metal Matrix Composites." *Acta Metall. Mater.* 1992; 40(9): 2361-2373.

31. Hanan, J. C., Aydiner, C. C., Ustundag, E., Swift, G. A., Kaldor, S. K., Noyan, I. C. "Characterization of Fiber/Matrix Interfaces Using X-Ray Microtopography." *Materials Science Forum.* 2002; 404-4: 919-923.

32. Bale H. A., Hanan J. C., Tamura N. , "Average and Grain Specific Strain Resolved in Many Grains of a Composite Using Polychromatic Microbeam X-Rays." *Adv. X-Ray Anal.*, 49, 2005, in press.

33. Eshelby J. D., "The Elastic Interaction Of Point Defects", *Acta Metallurgica,* Volume 3, Issue 5, September 1955, Pages 487-490.

34. Sachs G. Z verein deut Ing 1928;72:734

35. Taylor GI. J Inst Met 1938;62:307.

36. Molinari A, Canova GR, Ahzi S. Acta Metall. 1987;35:2983.

37. Kröner E. Acta Metall 1961;9:155.

38. Hutchinson JW. Proc R Soc London 1970;A319:247.

39. Tiem S, Berveiller M, Canova GR. Acta Metall. 1986;34:2139.

40. Lebensohn RA, Tome´ CN. Acta Metall Mater. 1993;41:2611.

41. Bishop, Hill, *Phil. Mag*. 42, pp. 414-427 and pp. 1298-1307, 1957.

42. Armstrong R. W., Head A. K., "Dislocation queueing and fracture in an elastically anisotropic material", *Acta Metallurgica, Volume 13, Issue 7, July 1965, Pages 759-764.*

43. Chin G. Y., Nesbitt E. A., Williams A. J., "Anisotropy of strength in single crystals under plane strain compression**",** *Acta Metallurgica, Volume 14, Issue 4, April 1966, Pages 467-476.*

44. Ibnabdeljalil, M., Phoenix, S. L. "Creep-Rupture of Brittle-Matrix Composites Reinforced with Time-Dependent Fibers - Scalings and Monte-Carlo Simulations." *J. Mech. Phys. Solids*. 1995; 43(6): 897-931.

45. Beyerlein, I. J., Phoenix, S. L. "Statistics of Fracture for an Elastic Notched Composite Lamina Containing Weibull Fibers .1. Features from Monte-Carlo Simulation." *Eng. Fract. Mech.* 1997; 57(2-3): 241-265.

46. Depaolini E., Franchini C., Marino F., **"**Experimental evaluation and mathematical description of the state of anisotropy in polycrystalline materials**",** *Materials Chemistry and Physics, Volume 10, Issue 4, April 1984, Pages 331-342.*

47. Lester, H. H., Aborn, R. M., *Army Ordnance* 6**,** 120, 1925-26.

48. Tamura N., Padmore H.A., Patel J.R., "High spatial resolution stress measurements using synchrotron based scanning X-ray microdiffraction with white or monochromatic beam", *Materials Science and Engineering* A 399 (2005) 92–98.

49. Liu W., Ice G. E., Larson B. C.,Yang W.,Tischler Z. H., "Nondestructive three-dimensional characterization of grain boundaries by X-ray crystal microscopy", *Ultramicroscopy* 103, 2005, 199–204.

50. Noyan, I. C., Schadler, L. S., "Characterization of Inhomogeneous Elastic-Deformation with X-Ray Diffraction." *Metall. Mater. Trans. A*, 1994; 25A: 341-347.

51. Amorós, J. L., Buerger, M. J., Canut de Amorós, M., "The Laue Method", 1-4, 1975.

52. Wilson., A. J. C., *Elements of X-ray Crystallography*, Addison-Wesley, 1970.

53. Davis, T. J., "X-Ray Diffraction Imaging Using Perfect Crystals**",** Journal Of X-Ray Science And Technology 6**,** 317–342 (1996) Article No. 0021

54. Miura, Y., Ihara, K., Fukaura, K., "Dynamic recrystallization in Al single crystals revealed by rapid X-ray Laue method", Materials Science and Engineering A280 (2000) 134–138

55. Chung J. S., Ice, G. E., "Automated indexing for texture and strain measurement with broad band pass X-ray micro beams ", *Journal of Applied Physics*, Volume 86, No.9,1999.

56. Sheremetyev I. A., Turball A. V., Litvinov Y.M., Mikhailov M. A.; *Nucl. Instrum. Methods Phys. Res*. A 308, 451, 1991.

57. Ravelli R.B.G., Krabbendam A.M.F, Kroon, H., J., *J. Appl. Crystallogr*. 29, 270, 1996.

58. Wenk H. R., Heidelbach F., Chateigner D., Zontone F., *J. Synchrotron Radiation*. 4, 95,1997.

59. MacDowell A.A., Celestre R.S., Tamura N., Spolenak R., Valek B., Brown W.L., Bravman J.C., Padmore H.A., Batterman B.W., Patel J.R., "Submicron X-ray diffraction", *Nuclear Instruments and Methods in Physics Research* A 467–468 (2001) 936–943.

60. Tamura N., Padmore H.A., Patel J.R., "High spatial resolution stress measurements using synchrotron based scanning X-ray microdiffraction with white or monochromatic beam", *Materials Science and Engineering* A 399 (2005) 92–98.

61. Liu W., Ice G. E., Larson B. C., Yang W., Tischler J. Z., "Nondestructive three-dimensional characterization of grain boundaries by X-ray crystal microscopy", *Ultramicroscopy* 103 (2005) 199–204.

62. Margulies L., Lorentzen T., Poulsen H.F., Leffers T., "Strain tensor development in a single grain in the bulk of a polycrystal under loading", *Acta Materialia* 50, 2002, 1771–1779.

63. Young-Han Park, Hyo-Young Yeom, Hyung-Guen Yoon, Kwang-Woo Kim, "The π/2 Side-Reflection Laue Technique and the New Chart", *J. Appl. Cryst.,*1997, 30, 456-460.

64. A. L. Patterson, " *International Table of X- ray Crystallography*", (Kynoch Birmingham, 1959), Vol II, pp. 164-174.

65. Böhm J., Wanner A., Kampmann R., Franz H., Liss K.D., Schreyer A., Clemens H., "Internal stress measurements by high-energy synchrotron X-ray diffraction at increased specimen-detector distance", *Nuclear Instruments and Methods in Physics Research* B 200, 2003, 315–322

66. Ice G. E., Larson B.C., Chung J.S., Tamura N., Tischler J.Z., Budai J.D. and Yoon M., "X-ray Optics For Polycrystalline Microdiffraction", ORNL, Oak Ridge, TN 37830 USA 2000.

67. Mehan R. L., "Fabrication and mechanical properties of sapphire whisker/aluminium composites", *Journal of Composite Materials*, Vol 4, pp 90–101, January 1970.

68 Ice G.E., Larson B.C., Tischler J.Z., Liu W., Yang W., "X-ray microbeam measurements of subgrain stress distributions in polycrystalline materials", *Materials Science and Engineering A, 2005.*

69. Hanan J. C. , Bale H. A., Coles B., "Uniaxial Tensile/Compressive Load Frame for X-ray Specimens", Unpublished work, 2005.

70. Tamura N., MacDowell A. A., Spolenak R., Valek B. C., Bravman J. C., Brown W. L., Celestre R. S., Padmore H. A, Batterman B. W., Patel J. R., "Scanning X-ray micro

diffraction with submicrometer white beam for strain/stress and orientation mapping in thin films", J. Synchrotron Rad. (2003). 10, 137-143.

71. Reuss A. Z. Angew Math Mech. 1929; 9:49.

72. Ice G.E., Larson B.C., Tischler J.Z., Liu W., Yang W., "X-ray microbeam measurements of subgrain stress distributions in polycrystalline materials", *Materials Science and Engineering A, 2005.*

VITA

Hrishikesh Bale

Candidate for the Degree of

Master of Science

Thesis: POLYCHROMATIC MICRO X-RAY BEAM STRAIN ANALYSIS OF ALUMINUM SAPPHIRE COMPOSITE

Major Field: Mechanical Engineering

Biographical:

Personal data: Born in Belgaum, India, On August 01, 1980, the son of Ashok and Ashwini Bale.

Education: Received Bachelor of Engineering degree in Mechanical Engineering from Visweswaraiah Technological University, Belgaum, India in June 2002. Completed requirements for Master of Science degree with a major in Mechanical and Aerospace Engineering at Oklahoma State University in December 2005.

Experience: Graduate Research Assistant in Mechanical and Aerospace Engineering Department, Oklahoma State University, Stillwater, Oklahoma, January, 2004 – December, 2005. Graduate Teaching Assistant in Mechanical and Aerospace Engineering Department, Oklahoma State University, Stillwater, Oklahoma, August, 2003 – December, 2004.

Name: Hrishikesh Bale Date of Degree: December, 2005

Institution: Oklahoma State University Location: Stillwater, Oklahoma

Title of Study: POLYCHROMATIC MICRO X-RAY BEAM STRAIN ANALYSIS OF ALUMINUM SAPPHIRE COMPOSITE

Pages in Study: 79 Candidate for the Degree of Master of Science

Major Field: Mechanical Engineering

Scope and Methodology of Study:

The results of an experimental technique with an advanced procedure to measure strains using polychromatic X-rays are presented. The experimental technique is based on the Laue method of diffraction, which utilizes polychromatic X-rays. By illuminating a definite volume of a composite sample consisting of an aluminum matrix A356 and single crystal sapphire fiber, the strain distribution throughout the matrix and fiber is studied. An advantage of using polychromatic X-rays, over that of the monochromatic X-ray beam, is that the diffraction patterns are obtained from nearly all of grains as compared to the small fraction observed typically with monochromatic X-rays.

Findings and Conclusions:

The technique proves to be successful in measuring the residual strains and the strain response to applied stress with an accuracy of 200 micro-strains. Using diffraction patterns from the composite at multiple axial load situations, change in strains is obtained. Strain maps obtained from this technique prove to be helpful in demonstrating the actual grain morphology in 2D and the respective strain states in the form of strain contours for every individual grain. A distribution representative of the nature of residual strains is also obtained at multiple scales with respect to the microstructure. The results along with the 3D analysis will help validation and modification of constitutive models for composite failure.

ADVISER: Dr. JAY C. HANAN